



Published in final edited form as:

Dev Dyn. 2023 November ; 252(11): 1338–1362. doi:10.1002/dvdy.629.

A framework to identify functional interactors that contribute to disrupted early retinal development in *Vsx2* ocular retardation *J* mice

Amanda M. Leung¹, Mahesh B. Rao², Nathan Raju², Minh Chung², Allison Klinger², DiAnna J. Rowe², Xiaodong Li², Edward M. Levine^{1,2,*}

¹Department of Cell and Developmental Biology, Vanderbilt University, Nashville TN 37232

²Department of Ophthalmology and Visual Sciences, Vanderbilt University Medical Center, Nashville TN 37232

Abstract

Background: A goal of developmental genetics is to identify functional interactions that underlie phenotypes caused by mutations. We sought to identify functional interactors of *Vsx2*, which when mutated, disrupts early retinal development. We utilized the *Vsx2* loss-of-function mouse, *ocular retardation J (orJ)*, to assess interactions based on principles of positive and negative epistasis as applied to bulk transcriptome data. This was first tested *in vivo* with *Mitf*, a target of *Vsx2* repression, and then to cultures of *orJ* retina treated with inhibitors of Retinoid-X Receptors (RXR) to target *Rxrg*, an upregulated gene in the *orJ* retina, and gamma-Secretase, an enzyme required for Notch signaling, a key mediator of retinal proliferation and neurogenesis.

Results: Whereas *Mitf* exhibited robust positive epistasis with *Vsx2*, it only partially accounts for the *orJ* phenotype, suggesting other functional interactors. RXR inhibition yielded minimal evidence for epistasis between *Vsx2* and *Rxrg*. In contrast, gamma-Secretase inhibition caused hundreds of *Vsx2*-dependent genes associated with proliferation to deviate further from wild type, providing evidence for convergent negative epistasis with *Vsx2* in regulating tissue growth.

Conclusions: Combining *in vivo* and *ex vivo* testing with transcriptome analysis revealed quantitative and qualitative characteristics of functional interaction between *Vsx2*, *Mitf*, RXR, and gamma-Secretase activities.

Keywords

neurogenesis; lineage fidelity; microphthalmia; retina; RNA sequencing; epistasis; Chx10; Mitf; Retinoid X receptor; gamma secretase; Notch

*Corresponding author Ed.levine@vumc.org.

The authors declare no conflicts of interest

RNA sequencing datasets are deposited into the Gene Expression Omnibus Repository (GEO: GSE227056).

Ethics statement: All procedures and experiments with mice were approved under protocol M1500036 by the Vanderbilt Institutional Animal Care and Use Committee and conformed to the ARVO guidelines for the use of animals in vision research. The research was conducted in concordance with the NIH guidelines for Responsible Conduct in Research (RCR).

Introduction

Vsx2 is an evolutionarily conserved homeodomain transcription factor that with *Vsx1*, defines the *Visual System Homeobox* (VSX) class of homeobox genes¹. Mutations in human VSX2 cause bilateral congenital microphthalmia, disrupted retinal architecture, and lifelong blindness, abnormalities which are also present in *Vsx2* mutant mice^{2–6}. A definitive marker of retinal domain specification during regionalization of the optic vesicle, *Vsx2* is expressed in retinal progenitor cells (RPCs) throughout development, ultimately resolving to cohorts of bipolar cells and Müller glia⁷. During early retinal development, *Vsx2* regulates tissue identity (i.e. retinal), RPC proliferation, and the initiation of retinal neurogenesis^{2,8–12}. *Vsx2* also promotes optic cup morphogenesis in *medaka* and multipotentiality in zebrafish RPCs^{13,14}. The importance and conservation of VSX genes in visual system development is further exemplified by their roles in optic lobe formation in *Drosophila* and in *C. elegans*, where the VSX ortholog *Ceh-10* is a terminal selector gene for the AIY sensory interneuron, which is part of a light-responsive neural circuit in a related nematode species^{15,16}.

The functional requirements of *Vsx2* in early mouse retinal development are complex. Best studied with the recessive loss-of-function *ocular retardation J* allele (homozygotes are referred to as *orJ*), which encodes a premature stop codon in the *Vsx2* homeodomain, retinal identity is compromised as revealed by ectopic expression of genes normally restricted to RPE or ciliary epithelium^{2,8,17}. However, the retinal domain is still specified, optic cup morphogenesis occurs, and *Vsx2* mRNA (but not protein) remains expressed^{2,6,7,18,19}. Genetic analysis of the neomorphic DNA-binding defective mutant *Vsx2^{R227W}*, which exhibits a more severe phenotype than the *orJ* mutant, suggests that *Vsx2* ensures lineage fidelity, allowing the retinal gene expression program to occur in the absence of extra-lineage or cryptic gene expression programs⁶. RPC proliferation is greatly reduced in all existing *Vsx2* mouse mutants but nevertheless persists through retinal development and at least for the *orJ* retina, into adult stages^{9,10}. Neurogenesis occurs in the *orJ* retina but with a tissue-specific delay of about two days, initiating at ~E13.5^{2,6,11,12,20}. While these problems contribute to severely disrupted retina formation, these partial requirements highlight the complexity in how *Vsx2* regulates early retinal development. Adding to this complexity, the disruptions in lineage fidelity, proliferation, and neurogenic timing temporally overlap. Analysis of *orJ*<>wt chimeric embryos suggest that lineage fidelity, proliferation, and neurogenic timing are under cell autonomous regulation by *Vsx2*, but proliferation also has a non-cell autonomous component that could act in parallel to *Vsx2* or converge onto *Vsx2*-regulated genes^{20–22}. To the extent that these phenotypes are interconnected, either hierarchically or at the level of gene regulation, is not clear.

Previously identified functional interactors of *Vsx2* in mice and human organoids include genes such as *Mitf*, *p27Kip1*, and *Prdm1*, and signaling pathways such as FGF, Sonic hedgehog, and Wnt^{6,9,12,19,23–26}. Identification of these interactors has been accomplished with genetics or pharmacological testing and it is likely that additional interactors can be identified through these approaches.

In this study, we suppress the activities of candidate functional interactors in the *orJ* retina. Beginning with *Mitf*, we assessed its genetic impact on the initiation of neurogenesis by immunohistology and an assessment of phenotypic traits with RNA sequencing data using a classification system of gene regulatory dependencies combined with gene set overrepresentation analysis (ORA; see Suppl. File 1 for non-standard abbreviations and terms). We then treated E12.5 organotypic cultures of *orJ* retina and lens (hereafter referred to as *orJ* retinal explants) with small molecule inhibitors of two other candidate interactors, Retinoid X receptor gamma (*Rxrg*), a highly upregulated gene in the *orJ* retina, and gamma-Secretase (GS), an enzymatic activator of Notch signaling and key regulator of RPC proliferation and neurogenesis^{27,28}. In addition to immunohistology, functional interactions were assessed with bulk RNA sequencing and applying the logic of *positive* and *negative* epistasis to the observed changes in gene expression. As defined by Lehner²⁹, positive epistasis occurs when a second mutation decreases the phenotypic severity caused by the first mutation, and negative epistasis occurs when the phenotypic severity is increased. Positive epistasis has traditionally served as evidence for direct genetic interaction between two genes with one gene repressing the other as the simplest mechanism. Negative epistasis is more complicated because more severe phenotypes can arise through disruptions in separate mechanisms that are regulated independently by the genes under analysis, or through convergence onto mechanisms such as gene regulatory networks and/or signaling networks. We show here that *Mitf* exhibits partial, but definitive positive epistasis, that *Rxrg* does not appear to exhibit functional epistasis within the confines of our testing paradigm, and that GS activity exhibits convergent negative epistasis with *Vsx2* through regulation of genes associated with RPC proliferation. We propose that this approach provides sufficient resolution to expand and refine the *Vsx2* interaction network for early retinal development and could be adapted to other gene mutations with complex phenotypes.

Results

Analogous to *Vsx2* for the retinal domain, *Mitf* marks the RPE domain during optic vesicle regionalization and drives RPE differentiation^{30–32}. *Mitf* is initially expressed throughout the optic vesicle and its subsequent downregulation in the nascent retinal domain is *Vsx2*-dependent, consistent with it being a direct target of *Vsx2* repression^{6,26,33–36}. Loss of function and dominant negative mutations in *Mitf* suppress the mutant phenotypes of several *Vsx2* mutant alleles, and more severe phenotypes (hyperpigmentation, increased hypocellularity) occur when *Mitf* expression is enhanced^{6,8,17,37,38}. *Mitf* is therefore an excellent candidate to be the major driver of the traits and underlying gene expression changes that define the early retinal development phenotype in *Vsx2* mutants. Addressing this first provides the context for placing other functional candidates into the highest level of the *Vsx2* interaction network.

The *mi* allele partially rescues the delay in neurogenesis in the *orJ* retina

The delayed onset of neurogenesis offered a straightforward measure to assess the impact of reducing *Mitf* activity, and the gap of 2 days between neurogenesis onset in wild type (E11.5) and *orJ* retinas (E13.5) provided a window to distinguish between full or partial restoration of timing. Neurogenesis initiates in the central retina and progresses toward the

periphery over several days, thereby allowing evaluation of the pattern and progression. These features are easily tracked by the expression of Class III β -tubulin (Tubb3; Figure 1A–F, arrows indicate first incidence of Tubb3 staining; see Table 2: Primary antibodies), which is activated in RPCs as they exit the cell cycle and transition to postmitotic, neuronal precursor states^{39–41}.

The *Mitf* allele *mi* was used to generate combinatorial mutants. The *mi* mutation is a three-nucleotide deletion that reduces DNA binding, but dimerization with wild type Mitf protein and other interacting proteins still occur, conferring dominant-negative activity^{42,43}. For this reason, we used heterozygous mutants (*mi*^{het}), unless noted. As expected, neurogenesis initiated earlier in the *orJ*; *mi*^{het} retina compared to *orJ* (Fig. 1G–I; arrow in H). However, onset was still delayed by about 1 day compared to the wild type retina indicating a partial restoration in timing. This partial rescue could be due to the persistence of Mitf activity or related factors (see discussion). Indeed, more severe phenotypes are observed in *mi* homozygotes (*mi*^{homo}) or in combinatorial *Mitf* mutant mice^{42,44,45}. We therefore examined the *orJ*; *mi*^{homo} retina for further correction of the neurogenic delay. The delay persisted at E11.5 (Fig. 1J), but Tubb3 expression was evident at E12.5 and E13.5 (Fig. 1K,L). Tubb3+ cells were found in the *mi*^{het} retina at E11.5, but the limited number of cells suggests that the onset of neurogenesis did not occur earlier than the wild type retina, which argues against the idea that improved timing was due to an indirect effect of the *mi* mutation on RPE to retina signaling (Fig. 1M–O).

To quantify these observations, measurements were done for neurogenic progression (Fig. 1P) and neurogenic output (Fig. 1Q). Neurogenic progression was calculated as the percentage of the retina expressing Tubb3 along a line extending along the central to peripheral axis of the retina and neurogenic output was inferred from the ratio of Tubb3+ pixels to total pixels in the neurogenic region (see Experimental Procedures). As expected, neurogenic progression lagged in the *orJ* retina but was improved in the combinatorial mutants, with the *orJ*; *mi*^{homo} retinas similar to wildtype at E13.5 (Fig. 1P; see Suppl. File 2 for statistics). Neurogenic output was impaired in *mi*^{het} and *orJ* retinas relative to wild type, but the *orJ*; *mi*^{het} and *orJ*; *mi*^{homo} mutants showed improvements by E13.5 (Fig. 1Q; see Suppl. File 2 for statistics). These observations align with prior findings that the *orJ* and *mi* alleles exhibit positive epistasis, but they also suggest that *Mitf*-independent factors contribute to the *orJ* phenotype.

***Mitf* partially accounts for the gene expression changes caused by the absence of *Vsx2*.**

To gain a transcriptome-wide view of the changes caused by the *orJ* and *mi* mutations, we performed RNA sequencing on E12.5 retinas from *orJ*^{het} (control), *orJ*, and *orJ*; *mi*^{het} mice. This age captures the neurogenic delay in the *orJ* retina as well as improvements caused by the *mi* allele. *orJ*^{het} mice exhibit normal retinal development¹¹ and a pilot microarray experiment comparing *orJ*^{het} and wild type retinas revealed highly similar gene expression profiles (unpublished observation). Library preparation and sequencing for all samples were done simultaneously, facilitating direct comparisons of gene expression across the 3 genotypes (Fig. 2A). Principal components analysis revealed that most of the variance between datasets correlated with genotype (Fig. 2B). The *orJ*; *mi*^{het} samples clustered

between the control and *orJ* samples but were closer to *orJ* on the first principal component axis, indicating that reducing *Mitf* activity did not restore the transcriptome-wide expression profile to a wild type state but that the overall trend was towards restoration.

DESeq2 was used to identify differentially expressed genes (DEGs) by pairwise comparisons across the three genotypes (Fig. 2C; Suppl. File 3). 14073 genome mapped features (GMFs) were identified and after applying a false discovery rate (FDR) cutoff of 0.01 (equivalent to adjusted p-value), 5195 DEGs were identified in the *orJ* retina when compared to control (OvC), 949 DEGs were identified in the *orJ; mi^{het}* retina compared to *orJ* (OMvO), and 3380 DEGs were identified in the *orJ; mi^{het}* retina compared to control (OMvC). Like the PCA analysis, the varying degrees of differential gene expression between genotypes suggest that the *orJ; mi^{het}* retina is more like *orJ* than wild type.

Partitioning of genes based on *Vsx2* and *Mitf* dependence.

We generated a classification system based on a gene's probability of being differentially expressed in the *orJ* and *orJ; mi^{het}* mutants (Table 1). Two FDR cutoffs were applied resulting in three broad categories: Genes with a p_{adj} value of ≤ 0.01 were assigned a DEG status of 'yes' (DEG-Y) indicating a DEG with high confidence, 'possible' (DEG-P) with a p_{adj} value in the range of >0.01 and ≤ 0.05 indicating low confidence in the DEG designation, and 'no' (DEG-N) with a p_{adj} value >0.05 (Table 1; Suppl. File 3). DEG status in the OvC comparison defined a gene's dependency on *Vsx2* and each gene was assigned to a *Vsx2* gene set: V1 for DEG-Y genes, V2 for DEG-P genes, and V3 for DEG-N genes (Table 1). Except where noted, analyses were focused on the *Vsx2*-dependent genes (V1 gene set).

With *Vsx2*-dependencies defined, the impact of *Mitf* on gene expression was assessed. DEG status in the OMvO comparison defined a gene's dependency on *Mitf* (Table 1; Suppl. File 3) and applying this as a filter to the V1 gene set (Fig. 2D) revealed simple regulatory relationships that are divided into three states of *Mitf* dependency: dependent (D), possibly dependent (pD), and independent (I). DEG status in the OMvC comparison was not informative on its own with respect to *Vsx2* or *Mitf* regulation (Table 1), but when applied as an additional filter, the extent of *Mitf* regulation could be inferred. This resulted in a more nuanced classification scheme with up to 6 distinct genes sets based on *Mitf* dependency, defined as V1.M1 through V1.M6 (Fig. 2E; similar classifications for the V2 and V3 genes are provided in Suppl. File 4). For V1.M1 genes, the changes in expression due to *Vsx2* loss of function are predicted to be fully dependent on *Mitf*, whereas V1.M3 genes are predicted to be partially dependent on *Mitf*, suggesting additional factors contribute to their differential expression. V1.M2 genes are also *Mitf*-dependent but distinguishing between full- or partial-dependence is less certain because of their DEG-P status in either the OMvO or OMvC comparisons. This is also true for V1.M4 genes but ambiguity lies in whether they are *Mitf*-dependent or -independent. V1.M5 genes are predicted to be *Mitf*-independent, and this gene set accounts for the largest cohort (44%) of *Vsx2*-dependent genes, in keeping with the partial restoration of the *orJ* phenotype by the *mi* mutation. The dependency of the V1.M6 genes on *Mitf* was deemed inconclusive because their DEG status in the

two comparisons with the OM dataset resulted in low-confidence or ambiguous regulatory predictions (i.e., DEG-P in OMvO and OMvC, or DEG-N in OMvO and OMvC).

Focusing on the *Mitf*-dependent genes (V1.M1, V1.M2, and V1.M3 gene sets), we predicted these genes would show improved expression in the *orJ; mi^{het}* mutant, trending back towards control levels. Indeed, 993 of 1004 genes (98.9%) exhibited this behavior. Because this aligns well with positive epistasis at the genetic level, this can be considered evidence of positive epistasis at the level of gene expression. Since very few genes exhibited worsened expression (i.e., greater divergence from wild type expression in the *orJ; mi^{het}* retina compared to the *orJ* retina), the incomplete rescue was unlikely to be due to aberrant effects of the *mi* mutation. Rather, it supports the hypothesis that additional factors contribute to the *orJ* phenotype.

It is also possible that *Mitf* may regulate the expression of genes that are not regulated by *Vsx2* (i.e., *Mitf*-dependent genes in the V3 gene set). This is an important consideration because *Mitf* is expressed at low levels in the embryonic retina³⁸ and a role for *Mitf* in regulating retinal gene expression could complicate a phenotypic assessment of the epistatic interaction between *orJ* and *mi*. Of the 7448 V3 genes, only 35 exhibited *Mitf* dependency (V3.M1 gene set; Suppl. File 4), indicating that *Mitf* has a minor impact on the expression of *Vsx2*-independent genes. Despite this low number of genes, the *mi* mutation could promote a compensatory factor and one candidate is *Cyclin D2 (Ccnd2)*, a *Vsx2*-independent gene that is upregulated in the *orJ; mi^{het}* retina (Suppl. File 3) that promotes cell cycle progression and regulates neurogenic output in the ciliary margin⁴⁶.

Designation of gene regulatory circuits for V1 genes based on *Mitf*-dependency

The high degree of positive epistasis at the level of gene expression allowed us to generate gene regulatory circuits (GRCs for the *Vsx2*- and *Mitf*-dependent genes of the highest confidence, specifically those in the V1.M1, V1.M3, and V1.M5 gene sets (Fig. 3). Considering the directional changes in differential expression (DE) in the three pairwise comparisons (OvC, OMvO, OMvC), 6 GRCs were identified with a major subdivision based on whether *Vsx2* promotes or inhibits expression, designated as V1p or V1i, respectively. In general, *Mitf*-dependent genes skewed toward GRCs based on *Vsx2* inhibition (V1i.M1, V1i.M3) whereas a more balanced GRC distribution was observed for *Mitf*-independent genes (V1i.M5, V1p.M5). This is consistent with the idea that *Mitf* promotes expression of non-retinal genes to a greater extent than it inhibits the expression of retinal genes. Since differentially expressed transcription factors (DETFs) could be candidates for extending the *Vsx2*-interaction network, DETFs were identified for each GRC with the top 2 ranked DETFs listed (Fig. 3). In general, the number of DETFs increased with the size of the DEG pool except for the V1p.M5 GRC, which has a similar number of DETFs as the V1i.M3 and V1p.M3 GRCs despite a much larger number of DEGs overall (1184 compared to 215 and 474, respectively). This could reflect a more direct role for *Vsx2* in promoting genes that are *Mitf*-independent. Interestingly, the top DETFs in the *Vsx2*-promoting GRCs have established roles in promoting retinal development, and neurogenesis in particular^{47,48}.

Overrepresentation analysis reveals *Mitf*-dependent and -independent impacts on curated molecular pathways.

Functional annotation of DEGs was done with Ingenuity Pathway Analysis (IPA; Qiagen). We utilized the Canonical Pathways function which performs an overrepresentation analysis (CP-ORA) of curated collections of genes that are components of signaling, metabolic, and other defined molecular pathways⁴⁹. The p-value for each pathway was calculated with the right-tailed Fisher's exact test and an alpha level of 0.05 was used to reject the null hypothesis – that overrepresentation or enrichment of a pathway in the query data is due to random chance. The antilog of the p-value was used for visualization purposes and is referred to as the ORA score. An ORA score of 1.3 is equivalent to $p = 0.05$; larger ORA scores are equivalent to smaller p-values. IPA also calculates a Z-score (activation Z-score) to predict whether a pathway is likely to be activated or inhibited from the gene expression data. Activation Z-scores greater than 2 predict activated pathways and less than -2 predict inhibited pathways⁴⁹. Pathways can also lack activation Z-scores, due to insufficient information from the gene expression data or lack of pathway topology.

CP-ORA was done for five DEG sets: V1.ALL (the full cohort of V1 genes), V1.M1-M3 (all *Mitf*-dependent genes), V1.M1 (V1 DEGs fully dependent on *Mitf*), V1.M3 (V1 DEGs partially dependent on *Mitf*), and V1.M5 (V1 DEGs that are *Mitf*-independent; tabulated results in Suppl. File 5). As expected, the number of overrepresented pathways increased with the number of genes in each DEG set (tabulated results in Suppl. File 6). To compare pathways by their dependencies on *Vsx2* and *Mitf*, the two pathways with the highest ORA scores for each DEG set were identified and their ranks by ORA score across the 5 DEG sets were assessed (Fig. 4; Suppl. File 6). 6 pathways were identified (Fig. 4A). All have significant ORA scores in the V1.ALL DEG set (Fig. 4B) and 5 of the 6 pathways have significant scores in the gene set containing all *Mitf*-dependent genes (V1.M1-M3; Fig. 4C). The *Kinetochores Metaphase Signaling (KMS)* and *Breast Cancer Regulation by Stathmin1 (BCRS)* pathways are associated with microtubule dynamics, mitosis, and cell cycle control, and are overrepresented in the V1.M3 and V1.M5 gene sets, but not in V1.M1 (Fig. 4D–F). Their activation Z-scores suggest that the *KMS* pathway was inhibited and the *BCRS* pathway was activated, consistent with inhibited mitosis and cell cycle progression (Fig. 4G,H). The *Phagosome Maturation (PM)* and *Iron Homeostasis Signaling (IHS)* pathways are important for rod outer segment turnover and iron regulation in RPE^{50,51}, respectively, and both are overrepresented in the V1.M1 gene set, indicative of strong *Mitf*-dependency (Fig. 4C–F). The *LPS/IL-1 Mediated Inhibition of RXR Function (RXRi)* pathway was overrepresented in the V1.M3 gene set and its activation Z-score is consistent with inhibition (Fig. 4C–F,I). Since *Rxrg* is a V1.M3 gene and the highest ranked upregulated DEG in the *orJ* retina, the presence of the *RXRi* pathway suggests elevated RXR activity. The *Transcriptional Regulatory Network in Embryonic Stem Cells (TRNESC)* was the only pathway to be specifically overrepresented in the V1.M5 set (Fig. 4D–F), consistent with the high number of DETFs in the V1.M5 GRCs (Fig. 3).

Mitf partially accounts for lineage infidelity in the *orJ* retina.

Although IPA identified several gene ontology (GO) terms and disease categories corresponding to disrupted eye development and congenital CNS abnormalities (not shown),

direct insight into potential effects on lineage fidelity were not forthcoming. This likely reflects a lack of contextual information in the Ingenuity Knowledge Base, an issue that could also apply to other broadly used knowledge databases. We predicted that ORA using lists comprised of genes specific to the nascent neural retina (NR) and RPE tissues would resolve this. We used the *My Lists* feature in IPA, which employs the same statistical modeling as CP-ORA, but for user-generated gene lists. To avoid subjectively selecting genes, we generated gene lists from RNA sequencing data produced from self-organizing mouse optic cup cultures that were treated for 5 days with Fibroblast Growth Factor 2 to generate neural retina-fated tissue (NR) or CHIR99201 (Wnt/b-catenin pathway agonist) to generate RPE-fated tissue (Andrabi 2015). We selected the most differentially expressed genes between them, aiming for approximately 100 genes in each list that were also present in our dataset (Fig. 5A; Suppl. File 7; see Experimental Procedures for method and parameters).

ORA for the V1.ALL gene set revealed high ORA scores for the NR and RPE gene lists, suggesting that they provide good representation of both tissue states in the cohort of *Vsx2*-dependent genes (Fig. 5B, Suppl. File 8). ORA for *Mitf*-dependent genes (V1.M1, V1.M2, V1.M3) produced significant scores for the NR and RPE lists with a higher ORA score for RPE (Fig. 5B). Comparison of the ORA scores for the V1.M1, V1.M3, and V1.M5 gene sets revealed a trend away from *Mitf*-dependence for the NR genes and a trend toward *Mitf*-dependence for the RPE genes (Fig. 5C). Identifying the GRCs to which the NR and RPE genes belong confirmed these trends with most of the RPE genes in the V1i GRCs and the NR genes in the V1p GRCs (Fig. 5D,E). These observations further support the idea that *Mitf* negatively impacts lineage fidelity by promoting the expression of nonretinal genes to a greater extent than by repressing retinal genes.

***Mitf* activity is not a major factor in disrupting neurogenesis in the *orJ* retina**

We applied similar logic to determine how genes associated with retinal neurogenesis and retinal cell types were distributed. Gene lists were generated through differential gene expression analysis of a single cell atlas of mouse retinal development⁵². The analysis was limited to cells harvested at E11.5, E12.5, and E14.5 to generate gene lists for developmentally relevant cell types: early RPCs (eRPC), neurogenic RPCs (nRPC), RGCs, amacrine cells (Ama), horizontal cells (HC), cones (C), photoreceptor precursors (PhPr), and an aggregated non-retinal cell types grouping (RPE_M_O) that includes RPE, ciliary margin, lens epithelium, and periocular mesenchyme⁵². As with the NR and RPE lists, we aimed for approximately 100 genes from each list to be present in our dataset although this was not achieved for several lists (Fig. 6A; Suppl. File 9; see Experimental Procedures for parameters and method). This was largely due to a high number of shared genes between the Cone photoreceptor (C) and Photoreceptor precursor (PhPr) gene lists and the Amacrine (A) and Horizontal cell (HC) gene lists. In these cases, the gene lists were merged (C_PhPr and A_HC). Other genes that were found in more than one cell type were excluded from all cell types except for *Asc11*, which was assigned to the nRPC list (Suppl. File 9).

ORA for the V1.ALL gene set produced significant scores for all cell types except the RPE_M_O list (Fig. 6B; tabulated data for all gene sets analyzed in Suppl. File 10). The

ORA score for nRPC genes was highest, suggesting that *Vsx2* regulates many genes in nRPCs, or more generally, the nRPC state, which would be consistent with the delayed onset of neurogenesis. ORA was then done for the different V1 gene sets and the V1.M5 genes consistently produced the highest ORA scores for each cell type (Fig. 6C). *Mitf* is also likely to affect nRPC gene expression since the ORA scores were significant for the V1.M1-M3 and V1.M3 gene sets (Fig. 6C (nRPC graph)). Cone_PhPr genes were also overrepresented in the V1.M1-M3 set (Fig. 6C, Cone_PhPr graph). Gene distributions by GRC showed a skew toward V1p GRCs for nRPC and RGC genes and more even distributions between V1p and V1i GRCs for eRPC, Cone_PhPr, and A_HC genes (Fig. 6D). The unexpected outcome of retinal cell type genes being inhibited by *Vsx2* could be because they are also expressed in RPE (i.e., *Crx*) or other non-retinal tissues, or are expressed prematurely in *orJ*RPCs (i.e., *Crx*, *Rxrg*). In sum, the gene lists used to represent each cell type correlate well the delay in neurogenesis and support the hypothesis that *Mitf* partially contributes to the delay in the onset of neurogenesis in the *orJ* retina.

Inhibition of RXR activity in *orJ* retinal explant culture reveals *Rxrg* to be a minor functional interactor with *Vsx2*.

That *Mitf* activity only partially accounts for the *orJ* phenotype reveals the pleiotropic nature of *Vsx2* interaction network at its highest level and suggests additional factors interact with the *orJ* allele to promote the mutant phenotype as well as to set the degree of phenotypic severity. The most direct approach to identify functional interactors is by genetic suppression of candidate factors *in vivo* as done for *Mitf*, but this is not easily done because of the limited availability of mutant alleles and the significant effort needed to generate combinatorial mutants. We therefore treated E12.5 *orJ* retinal explant cultures with small molecules to inhibit the activities of candidate interactors (see Experimental Procedures).

Our first focus was on *Rxrg*, the highest ranked DEG by adj-p-value in the OvC comparison (Suppl. File 3). Antibody staining confirmed the increase in *Rxrg* expression with a broad distribution across the E12.5 *orJ* retina (Fig. 7A). *Rxrg* is a nuclear receptor that binds to 9-cis retinoic acid and regulates transcription of target genes as a homodimer or in heterodimer combinations with other nuclear receptors that include the retinoic acid receptors (RARs), liver X receptors (LXRs), and thyroid hormone receptors (TRs)⁵³. *Rxrg* is normally expressed in RGCs and cones^{54–57}, but the delay in neurogenesis suggests that its ectopic expression in *orJ*RPCs is not due to the differentiation of these cell types. *Rxrg* is also transiently expressed in the nascent RPE at E10.5 and at the peripheral border between the NR and RPE⁵⁸, suggesting that it could contribute to lineage infidelity in the *orJ* retina. Its pattern of DE places it in the V1i.M3 GRC (Fig. 3E), suggesting that *Mitf* partially contributes to its upregulation. Based on these data, we hypothesized that *Rxrg* activity is an additional factor in causing the *orJ* phenotype and suppressing its activity will exhibit positive epistasis with the *orJ* allele.

E12.5 *orJ* retinal explants were treated for 24 hr with HX531 (Table 3: Small molecules), a highly selective small molecule inhibitor of RXR activity (IC₅₀: 18nM)⁵⁹. Contrary to our prediction, we did not observe changes in EdU incorporation or in the expression of Hes1, Neurogenin 2, or Tubb3, which mark proliferation, RPCs, nRPCs and postmitotic

neuronal precursors, respectively (data not shown). This suggested that RXR activity, and by inference, *Rxrg*, is not a strong interactor in promoting the *orJ* phenotype at E12.5, despite its ectopic expression.

RNA sequencing was done to determine the effect of HX531 treatment on gene expression. 19321 GMFs were mapped and 67 DEGs were identified (27 upregulated, 40 downregulated) with an FDR cutoff of 0.05 (Fig. 7B; tabulated data in Suppl. File 11). qPCR was done for the 3 top DEGs (defined by adj-pval; Suppl. File 11); the ATP-binding cassette transporters *Abca1* and *Abcg1*, and the Stearoyl-CoA desaturase *Scd2*. A significant effect was not observed for *Abcg1*, but *Abca1* and *Scd2* were downregulated by HX531 treatment, consistent with the RNAseq data and with RXR regulation in other contexts^{60,61}. CP-ORA with the HX531 DEGs identified overrepresented pathways associated with RXR signaling (Fig. 7C; tabulated data in Suppl. File 12). These same pathways were identified by CP-ORA in the *orJ* and *orJ;mi^{hbet}* mutants (referred to as the *mutants* dataset; Fig. 7E; Fig 4, gray bars; tabulated data in Suppl. File 5), but only the *LXR/RXR Activation* and *RXRi* pathways were significant in the full cohort of *Vsx2*-dependent genes (V1.ALL; Fig. 7E). However, ORA with the NR, RPE, and retinal cell type gene lists in the *HX531* dataset revealed overrepresentation for the NR gene list in the HX531 DEGs, but with only 3 genes (tabulated results in Suppl. File 13). These observations suggest that HX531 treatment had a measurable effect with respect to RXR activity, but not on retinal identity, proliferation, or neurogenesis.

We next examined the expression characteristics of the HX531 DEGs but in the context of the *mutants* dataset. 35 of the HX531 DEGs were *Vsx2*-dependent (V1 genes), 5 were possibly dependent (V2 genes), 12 were *Vsx2*-independent (V3 genes), and 15 were absent from the *mutants* dataset, leaving a total of 52 genes for cross comparisons between the *HX531* and *mutants* datasets (Fig. 7F; tabulated data in Suppl. File 14). To assess epistasis at the level of gene expression, the 52 HX531 DEGs were parsed by their directional changes in gene expression (DE) in both datasets (Fig. 7G; Suppl. File 14). Eighteen genes changed in opposite directions, indicative of positive epistasis (sum of underlined numbers), and 24 genes changed in the same direction, indicative of negative epistasis (sum of italicized numbers). The roughly even split precluded a prediction of one type of epistasis over the other. The 12 HX531 DEGs that were *Vsx2*-independent is consistent with RXR activity having a non-epistatic relationship with *Vsx2*, and likely in a *Rxrg*-independent manner. In this regard, *Rxra* and *Rxrb* are expressed in the E12.5 retina⁵⁸, remain expressed in the E12.5 *orJ* retina (Suppl. File 3), and *Rxra* knockout mice have ventral growth defects and coloboma in the embryonic retina^{62,63}. A reasonable prediction is that the *orJ; Rxra* double mutant phenotype would be more severe than the single mutants due to independent, additive effects.

With respect to *Mitf* regulation, the 35 HX531 DEGs that were identified as V1 genes in the *mutants* dataset are distributed across all categories of *Mitf*-dependence (Fig. 7H), but ORA of these DEGs in the *mutants* dataset revealed that overrepresentation was confined to the V1.M1 (full *Mitf*-dependence), and V1.M3 (partial *Mitf*-dependence) gene sets (Fig. 7I; tabulated data in Suppl. File 15). This suggests that *Mitf* also has a role in regulating genes that are dependent on RXR activity, but the interaction with *Mitf* is likely to be complex. To

illustrate this point, we consider the predicted GRC topologies for *Abca1* (Fig. 7I) and *Scd2* (Fig. 7J). Since *Abca1* expression was inhibited by HX531 treatment, it is predicted to be *promoted* by RXR activity, and this is referred to as *RXRp* for GRC topology. Like *Rxrg*, the increased expression of *Abca1* in the *orJ* retina is partially *Mitf*-dependent (V1.M3), and based on the RNA seq data (Suppl. File 3) and published *in-situ* hybridization data (GenePaint.org,⁶⁴), *Abca1* is likely to be expressed at a low level in the wild type retina. Taken together, the resulting GRC (V1i.M3::RXRp; Fig. 7I) places *Rxrg* and *Mitf* as likely regulators of *Abca1* expression in the *orJ* retina and is an example of a positive epistatic regulatory interaction. *Scd2* expression, on the other hand, is promoted by both *Vsx2* and RXR activity, and its reduced expression in the *orJ* retina is fully *Mitf*-dependent (V1.M1). The resulting GRC topology is V1p.M1::RXRp (Fig. 7J), which raises the question of how *Rxrg* could contribute to its regulation? Considering that *Scd2* is abundantly expressed in the wild type retina (Suppl. File 3; GenePaint.org,⁶⁴), it's unlikely that *Rxrg* caused its expression to decrease in the *orJ* retina. Rather, *Rxra* and/or *Rxrb* are better candidates for promoting *Scd2* expression resulting in a GRC that predicts a convergent negative epistatic regulatory interaction with *Vsx2* and *Mitf* (Fig. 7J). In sum, while our data show that regulatory interactions at the level of gene expression can be predicted, we propose that *Rxrg*, and RXR activity in general, is not a major driver of the early retinal *orJ* phenotype.

Inhibition of gamma-Secretase activity reveals convergent regulation of *Vsx2*-dependent genes associated with cell cycle progression and mitosis

We next focused on what could account for the delay in the onset of neurogenesis, and we reasoned that active Notch signaling could be a factor. Overexpression of the *Notch1* intracellular domain (NICD) preserves the RPC state at the expense of neurogenesis^{65–68}, and inhibiting Notch signaling promotes neurogenesis at the expense of RPCs^{27,28,69–71}. These effects are consistent with Notch signaling acting as a progenitor maintenance pathway and could account for the delayed neurogenesis in the *orJ* retina. Elevated Notch signaling could also account for the persistence of *orJ*RPCs despite their reduced rate of proliferation.

CP-ORA for all *Vsx2*-dependent genes (V1.ALL) in the *mutants* dataset identified Notch signaling as an overrepresented pathway, but the activation Z-score was too low to predict activity (Suppl. File 5). This is likely due to changes in expression of Notch pathway genes that are consistent with both activation and inhibition (tabulated data in Suppl. File 16). For example, the expression of the ligand genes *Dll1* and *Dll4* was reduced in the *orJ* retina, but *Jag2* was upregulated. Expression of *Notch1* receptor was reduced but *Notch2* was upregulated and *Notch3* was expressed but unaffected. The expression of *Hes5*, a functional readout of Notch signaling, was strongly reduced suggesting inhibited Notch signaling, but *Hes1* was unaffected, and *Hey2* was upregulated. Thus, although Notch pathway gene expression was altered in the *orJ* retina, signaling status was ambiguous.

A common pharmacological approach to block Notch signaling is with gamma-Secretase (GS) inhibitors^{72,73}. Intracellular cleavage of Notch receptors by GS generates the NICD isoform which translocates to the nucleus to regulate target gene expression. Although GS activity is not specific to Notch signaling⁷⁴, treatment of retinal explants or organoids at the

early stages of retinal neurogenesis with the GS inhibitor DAPT caused RPCs to rapidly exit the cell cycle and transition into RGC and cone photoreceptor precursors, effects that align well with genetic models of abrogated Notch signaling^{27,28,69–71}. Since the components of the GS complex are expressed in the *orJ* retina (Suppl. File 17), we predicted that GS inhibition would inhibit proliferation and accelerate the onset of neurogenesis in the *orJ* retina.

We treated E12.5 *orJ^{het}* (control) retinal explants for 24 hr with 1 μ M dibenzazapine (DBZ; Table 3: Small molecules), a potent GSI, for 24 hr. Retinal neurogenesis is underway by E12.5 and serves as a positive control since it overlaps with other studies incorporating DAPT treatment (Table 3: Small molecules)^{27,28}. As expected, precocious neurogenesis was observed (Fig. 8A, left panels), demonstrating reproducibility with prior studies (5 μ M DAPT gave similar results; not shown). We next treated E14.5 *orJ* retinal explants with 1 μ M DBZ and neurogenesis was also observed, demonstrating that *orJ* RPCs exhibit similar responses to GS inhibition after neurogenesis begins in the *orJ* retina (Fig. 8A, middle panels). However, we observed cytotoxicity with 1 μ M DBZ (and 5 μ M DAPT) in E12.5 *orJ* explants as indicated by pyknotic nuclei in the retina and lens (Fig. 8A, right panels). Lowering DBZ to 300 nM reduced pyknosis but precocious neurogenesis was not observed, even in E12.5 wild type retina (not shown). However, EdU incorporation was reduced in the E12.5 *orJ* retina and quantifications confirmed this with 300 nM DBZ and 1 μ M DAPT (Fig. 8B). This suggests GS activity promotes proliferation in *orJ* RPCs, but the lower concentrations of DBZ and DAPT precluded an assessment of GS inhibition on accelerating neurogenesis onset in the *orJ* retina.

RNA sequencing and differential gene expression analysis was done for 300 nM DBZ or vehicle treated E12.5 *orJ* explants (tabulated data in Suppl. File 18). Of the 19290 GMFs identified, 376 genes were differentially expressed based on an FDR cutoff of 0.01 (DBZ DEGs; Fig. 8C). This is notably higher than HX531 treatment, where 67 DEGs were identified with a less stringent FDR cutoff (0.05). 317 of the 376 DBZ DEGs exhibited decreased expression, indicating that GS activity generally promotes gene expression in the *orJ* retina. With respect to *Vsx2* regulation, 331 were *Vsx2*-dependent (V1 genes), 13 were possibly dependent (V2 genes), 29 were *Vsx2*-independent (V3 genes), and 3 were absent from the *mutants* dataset, yielding a total of 373 DEGs shared by the *mutants* and *DBZ* datasets (Fig. 8D). Partitioning of these DEGs by their directional changes in gene expression (DE; tabulated data in Suppl. File 19) in the 2 datasets revealed that 336 genes changed in the same direction (Fig. 8E, sum of italicized numbers). In contrast, only 8 genes changed in opposite directions (Fig. 8E, sum of underlined numbers), and 29 were only changed after DBZ treatment (V3 column). These observations indicate that DBZ treatment altered the expression of a large cohort of *Vsx2*-dependent genes in the same direction as the *orJ* mutation, suggesting that *Vsx2* and GS activity regulate a common set of genes in a similar manner. This convergence is strong evidence for negative epistasis.

We next determined the extent to which the DBZ DEGs receive input from *Mitf*. In contrast to the HX531 DEGs, which displayed a relatively flat distribution of genes across the V1 gene sets (Fig. 7E), DBZ DEGs in the *mutants* dataset were clustered into the V1.M3, V1.M4, and V1.M5 sets (Fig. 8F), which typify partial *Mitf* dependence (V1.M3) and

Mitf independence (V1.M5). ORA confirmed that this distribution was significant (Fig. 8G; tabulated results in Suppl File 20), and consistent with the observation that most of the DBZ DEGs exhibited decreased expression in the *orJ* retina or after DBZ treatment, the predominant GRCs are those in which both *Vsx2* and GS promote their expression (Fig. 8H).

CP-ORA was done for the DBZ DEGs in the *DBZ* dataset (DBZ DEGs_*DBZ* dataset) and the overlap of the top 5 pathways was compared to their ORA scores and rank from CP-ORA of all *Vsx2*-dependent genes in the *mutants* dataset (V1.ALL_*mutants* dataset; tabulated data in Suppl. Files 5 and 21). All 5 pathways in the DBZ DEGs_*DBZ* dataset analysis were associated with cell cycle control and mitosis (Fig. 8I, upper left graph), and all were identified as significantly overrepresented in the V1.ALL_*mutants* dataset analysis (Fig. 8I, upper right graph). Of note, the *KMS* pathway had the highest ORA score in both gene sets. The distribution of the activation Z-scores for the canonical pathways predicted inhibition with significant Z-scores for the *KMS*, *Cell Cycle Control of Chromosomal Replication*, *Mitotic Roles of Polo-like Kinase*, and *Estrogen-mediated S-phase Entry* pathways in both analyses (lower graphs in Fig. 8H). These trends are consistent with reduced proliferation, and the extensive overlap in the overrepresented pathways and their predicted inhibited states further supports the idea that *Vsx2* and GS promote RPC proliferation by promoting the expression of a large cohort of genes in a convergent manner and that GS activity exhibits negative epistasis with *Vsx2*.

ORA analysis of the DBZ DEGs in the *DBZ* dataset with the NR, RPE, and retinal cell type gene lists produced significant ORA scores for eRPC and nRPC genes with all identified genes (except one) reduced in expression (Fig. 8J; tabulated results in Suppl. File 22), placing these genes into V1p::GSp GRCs (Fig. 8K). Since ORA scores for retinal cell types other than RPCs were not significant, it is unlikely that DBZ treatment drove RPCs toward neurogenesis. Rather, most of the genes identified in the eRPC and nRPC gene lists are associated with cell cycle control and metabolism with the nRPC genes *FoxN4* and *Notch1* being notable exceptions (Suppl. File 23). *FoxN4* is a transcription factor required for generating amacrine and horizontal cell precursors and it promotes the expression of *Dll4*⁷⁵. Their reductions suggest that Notch signaling was inhibited by DBZ treatment, but more direct studies are required to assess this.

Discussion

We combined transcriptome profiling with *in vivo* and *ex vivo* interaction testing to assess the potential contributions of candidate genes and molecular activities to the early retinal phenotype of the *orJ* mutant mouse. The triangular experimental design used for the genetic transcriptome analysis enabled a semi-quantitative assessment of the gene regulatory and phenotypic impacts of *Mitf*, a direct target of *Vsx2* transcriptional repression. Our finding that *Mitf* activity only partially contributes to the early *orJ* phenotype established the context for identifying additional interactors. This led to the identification of *Rxrg*, a top ranked DEG in the *orJ* retina, but the weak effects of small molecule inhibition on RXR activity suggest that *Rxrg* has a minimal role in the phenotypic traits of the E12.5 *orJ* retina. We also determined that GS activity supports RPC proliferation in the absence of *Vsx2* by

sustaining expression, albeit reduced, of a large cohort of *Vsx2*-dependent genes in a manner consistent with convergent negative epistasis. This streamlined approach for interaction testing permitted straightforward assessments of candidate causal factors underlying a complex developmental phenotype (Fig. 9).

That *Mitf* exhibits positive epistasis with *Vsx2* was expected and the nearly complete concordance of improved expression for *Vsx2*-dependent genes by introduction of the *mi* allele gave us confidence that epistasis can be assessed at the transcriptomic level. Whereas the impact of the *mi* allele on alleviating the ectopic expression of non-retinal genes was anticipated, its relatively minor impact on the expression of retinal genes was not. Since the RNA sequencing data was generated with the *mi* allele in the heterozygous state, it is possible that wild type *Mitf* protein was still active in the *orJ; mi^{het}* retina. However, this issue had to be balanced with the potential for non-cell autonomous effects on retinal development from disruptions in RPE development caused by the *mi* allele in a homozygous state^{76–78}. Genetic redundancy is also possible since *Tfeb*, a related bHLH-zip gene, was upregulated in the *orJ* retina. These issues are somewhat mitigated with the *mi* allele since the mutant protein functions in a dominant negative manner by heterodimerizing with wild type *Mitf* and *Tfeb*⁴³, and because a large cohort of *Mitf*-dependent genes were identified. Even with the possibility of residual *Mitf* and/or *Tfeb* activity, our data suggest additional factors contribute to the *orJ* phenotype. Other ectopically expressed DETFs identified in the V1.M3, V1.M4, and V1.M5 gene sets are potential candidates, and their testing could reveal new hubs in the *Vsx2* gene regulatory network.

Despite its ectopic expression, *Rxrg* appears to have a minor role on its own, and this may hold true for the majority of candidate interactors. Of the genes affected by HX531 treatment, they were not correlated with the phenotypic traits of lineage fidelity, proliferation, or neurogenesis as suggested by the lack of overrepresentation in the context-specific gene lists. However, overrepresented canonical pathways were associated with RXR function. The directional changes in the expression of the HX531 DEGs and the distribution of *Vsx2* dependency suggests that HX531 impacted gene regulation by *Rxra* and/or *Rxrb* in addition to *Rxrg*. Based on predicted GRC topology, *Scd2* is one candidate for *Rxra* or *Rxrb* regulation, as are HX531 DEGs that were found to be *Vsx2*-independent. How this relates to *Vsx2* function in RPCs is not clear. It could reflect an altered metabolic state in *orJ*RPCs, especially as it pertains to cholesterol transport and/or lipid metabolism, of which *Abca1*, *Scd2*, and other HX531 DEGs have established roles^{60,79,80}. It could also reflect a role for *Vsx2* in controlling the timing of *Rxrg*-dependent gene expression such that it is activated when RPCs transition into RGC and cone precursors, the cells in which *Rxrg* is normally expressed and functions to establish the dorso-ventral distribution of S-cone photoreceptors in the mouse retina^{54–57}.

We acknowledge that concluding that *Rxrg* is not a strong interactor with *Vsx2* is only relevant for the specific conditions tested. For example, other than what was present in the fetal bovine serum, retinoids were not added to the culture medium, potentially causing reduced RXR activity in both the vehicle and HX531-treated cultures. Although this can't be excluded, adding retinoic acid could have had gain of function effects, further complicating the analysis. It is likely, however, that endogenous retinoids were

present in the culture since direct measurements in the embryonic mouse retina revealed high physiological concentrations that approached 500 nM⁸¹. Furthermore, the abrogated retinoic acid signaling observed in knockout mice for *Rdh10*, *Aldh1a1*, or *Aldh1a3*, three major retinoic acid synthesis enzymes, indicate that the retina is a major source of ocular retinoic acid after E10.5 (reviewed in^{82,83}). Importantly, these genes were expressed in the *orJ* retina, although *Aldh1a3* was reduced (Suppl. File 3). Ultimately, genetic tests of interaction could address these limitations.

Whereas *Rxrg* emerged as a candidate interactor from the RNA sequencing data of the *orJ* and *orJ;mi^{het}* mutants, our interest in GS activity arose from a prediction that inhibiting Notch signaling would accelerate the onset of neurogenesis in the *orJ* retina, a hypothesis based on prior knowledge of the function of Notch signaling and pharmacological GS inhibition in the embryonic retina and more recently in human retinal organoids⁸⁴. Although toxicity issues precluded us from testing this hypothesis, we found that GS inhibition with a low dose of DBZ further reduced RPC proliferation in *orJ*RPCs. This is not surprising since an established role for Notch signaling is to maintain stem/progenitor cells, but the extensive overlap and directional change in expression of GS-dependent genes with hundreds of *Vsx2*-dependent genes was unexpected. Importantly, it provides compelling evidence that the interaction of GS activity with *Vsx2* is one of negative epistasis where both support RPC proliferation by convergence onto a set of downstream genes. Convergent negative epistasis could also explain why RPCs persist and continue to proliferate (albeit slowly) in the *orJ* retina^{10,85}. Whether this is due to Notch signaling or another GS substrate is not clear but could be addressed by tests of interaction with Notch pathway components and/or GS substrates outside the Notch pathway⁷⁴.

In sum, with further testing of additional candidates, both in isolation and combination, it should be possible to identify factors that contribute to the *orJ* phenotype, whether acting independently of *Vsx2*, as minor or non-interactors, or as central hubs in a dynamic interactive network.

Experimental Procedures

Mice

All procedures and experiments with mice were approved under protocol M1500036 by the Vanderbilt Institutional Animal Care and Use Committee and conformed to the ARVO guidelines for the use of animals in vision research. 129S1 wild type mice (RRID:IMSR_JAX:002448) are used to maintain *Vsx2^{orJ}* mice. *Vsx2^{orJ}* mice (RRID:IMSR_JAX:000385) have been maintained in the lab for over 10 years with continual outcrossing to 129S1 wild type mice (RRID:IMSR_JAX:002448). *Mit^{mi}* mice were obtained from the Jackson Laboratories (Jax) on a C57Bl6 background and is currently maintained at Jax with the *Mit^{mi-wh}* allele (RRID:IMSR_JAX:000158). The *mi* allele has been maintained for over 6 years in our laboratory and continually crossed to *Vsx2^{orJ}* mice.

Tissue collection

Single night mating was used to generate embryos. The day of the plug was considered embryonic day 0.5. Embryos were collected at the following time points: E11.5, E12.5, E13.5 and E14.5. Embryos were staged using fore and hindlimb staging⁸⁶.

Tissue and Slide Preparation

Retinal explants and whole-head tissue were fixed in 4% PFA/PBS solution for 20 and 35 minutes, respectively. Following sucrose cryoprotection, samples were frozen in TissueTek OCT (Sakura Finetech) and stored at -80°C . 12 μm sections were adhered to Superfrost Plus slides (Fisher Scientific), dried on a warmer 37°C for 1–2 hr before storage at -20°C .

Immunohistochemistry

Slides were incubated in block solution (2% serum, 0.1% triton-x100, PBS pH 7.4) for 30–60 min at room temperature followed by primary antibody incubation overnight at 4°C overnight. After washing with PBS, sections were incubated with secondary antibodies in the dark for 2 hr at room temperature. DAPI (1:40000 in PBS) was added for 15 min. Slides were coverslipped with Fluoromount. EdU incorporation was detected with AlexaFluor 647 Click-iT Cell Reaction Kit (Invitrogen-Molecular Probes, Eugene, OR, USA).

Microscopy

Images were captured on a Zeiss LSM710 confocal microscope using the 40x water objective. Z-stack and tile scan was performed on each section to get a single image. Tile scanning was stitched online using the online stitching function during acquisition of each image using the Zeiss Zen software, and a composite of the z-stack was created in ImageJ/Fiji⁸⁷ using Image>Stacks>Max Projection.

Quantifications and statistical tests of neurogenic length, Tubb3 expression, and EdU incorporation

ImageJ/Fiji was used to obtain the retinal length using the freehand line tool to measure the inner edge of the retina (closest to the lens). The neurogenic region of the retina was defined by measuring the linear length of the tissue that Tubb3-positive cells occupied. The percentage of neurogenic length was calculated by dividing the neurogenic region by the retinal length and multiplying by 100. The Kruskal-Wallis test followed by Dunn's multiple comparisons test was used for statistical analysis (Suppl. File 2).

Neurogenic density was defined by ratio of Tubb3-positive pixels as a proxy for cells within the neurogenic region. This was measured by outlining region positive for Tubb3 staining and clearing the outside of the ROI using Edit>Clear Outside in ImageJ. Neurogenic regions were made binary with *Threshold* tool and *Analyze>Histogram* was used to count the number of positive (white) and negative (black) pixels. These values were used to produce the density within the neurogenic region by calculating the ratio of positive pixels over total pixels. For samples that did not display any positive beta tubulin staining, the % neurogenic length and Tubb3+ pixel ratios were set to 0. One-way ANOVA, Browne-

Forsythe test followed by Tukey's multiple comparisons test were used for statistical analysis (Suppl. File 2).

EdU was manually counted in a blinded manner using the multi-point tool in ImageJ. Area was determined by ROI selection of calibrated images using the measure function in ImageJ. One Way ANOVA and Tukey's multiple comparisons test was used for statistical analysis (Suppl. File 2).

Retinal Explant Culture

E12.5 *orJ* whole neural retina and lens were dissected away from the RPE and all other ocular tissues, transferred into 24-well plates, and cultured in 500 μ L of 1x DMEM/F12 (U.S. Biological, cat.# D9807-05), 1% FBS (ThermoFisher, cat.# 16140071), 1x N2-Plus supplement (R&D Systems, cat.# AR003), 33 mM glucose (Sigma, cat.# G7528), 1 mM Glutamax (ThermoFisher, cat.# 35050061), 1.3 mM NaHCO₃ (ThermoFisher, cat.# 25080094), 5 mM HEPES (ThermoFisher, cat.# 15630080), 100 U/ml Pen/Strep solution (ThermoFisher, cat.# 15070063). Control explants were treated with vehicle only (0.1% DMSO) and experimental explants were incubated with pan-RXR inhibitor (HX-531) or GSIs (DAPT and DBZ). Cultures were maintained for 24 hours at 37 degrees in a 5% CO₂ atmosphere. EdU (final concentration: 10 μ M) was added to the media for 30 min prior to the end of the culture.

RNA preparation, sequencing, and processing

For the *mutants* analysis, isolated retinal tissue was flash frozen in liquid N₂, and stored at -80°C. Upon thawing, samples were pooled (4 control, 6 *orJ*, 6 *orJ*; *m^{het}*) and total RNA was isolated with the RNeasy mini-Kit (Qiagen). Each pool was an independent replicate and 4 replicates per genotype were sequenced. Stranded mRNA libraries were prepared from RNA samples with a RIN of 7 or greater with the NEB Ultra II library kit.

For explant cultures, the lens was dissected away from the retina at the end of the culture period, flash frozen in liquid N₂, and stored at -80°C. Samples were prepped individually with Trizol (Invitrogen). A minimum of 3 replicates per condition were sequenced. Stranded mRNA libraries were prepared from RNA samples with a RIN of 7 or greater with the NEBNext® Single Cell/Low Input RNA Library Prep Kit.

150 bp paired end sequencing was done with the NovaSeq6000 S2 flow cell at the Vantage core facility (Vanderbilt University). Data processing was done by Creative Data Solutions (Vanderbilt University). Paired end raw FASTQ files were assessed for quality by FastQC (<https://www.bioinformatics.babraham.ac.uk/projects/fastqc/>) and TrimGalore (https://www.bioinformatics.babraham.ac.uk/projects/trim_galore/) respectively. Reads were aligned to the reference mouse genome mm10 (GRCm38) using Spliced Transcripts Alignment to a Reference (STAR) version 2.6⁸⁸ using GENCODE comprehensive gene annotations (Release M14) as a reference. Approximately 70% of the raw reads were uniquely mapped to the reference genome. HTSeq was used for counting reads mapped to genomic features⁸⁹ and pairwise differential gene expression analysis was performed using DESeq2⁹⁰

Bioinformatics Analyses

Preparation of the DESeq2 datasets in Supplemental Files:

Mutants dataset (Suppl. File 3): Gene metadata, log₂FC, adjusted p-values, the FDR rank based on the adjusted p-values, and the means of the normalized counts for each genotype were merged into a single file from each of the DESeq2 comparisons. Molecular function for each gene from IPA was also merged into the file. DEG designations for each gene in the pairwise comparisons were assigned based on two adj p-value cutoffs (red; see results). *Vsx2*- and *Mitf*-dependencies (orange) were assigned from the filtering method shown in Fig. 2 and Supplemental Figs. 1 and 2. *Vsx2* and *Mitf* gene sets were assigned as well as GRCs (blue). Genes that didn't fall into a GRC are indicated by #N/A.

HX531 dataset (Suppl. File 11): Gene metadata, log₂FC, adjusted p-values, rank based on the adjusted p-values, means of the normalized counts for each treatment and the mean expression of both treatments combined were retained. DEG designations were based on a single adj-p value cutoff (FDR) of 0.05, resulting in DEG-Y and DEG-N classifications (red).

DBZ dataset (Suppl. File 18): Gene metadata, log₂FC, adjusted p-values, rank based on the adjusted p-values, means of the normalized counts for each treatment and the mean expression of both treatments combined were retained. DBZ DEG designation was based on two adj-p value cutoffs (FDR) resulting in DEG-Y, DEG-P and DEG-N classifications (red).

Ingenuity Pathway Analysis (IPA)—The DESeq2 pairwise comparison tables were uploaded onto the Ingenuity server and the Core Analysis package was used to perform CP-ORA, ORA, and pathway topology analysis⁴⁹. The reference genome for CP-ORA and ORA were the dataset themselves as opposed to the complete mouse genome. Statistics (Fishers exact test, Z-score algorithm) were done on specified subsets of genes from the datasets and referred to in IPA as *analysis ready molecules* (ARMs). ARMs based on *Vsx2*- and *Mitf*-dependencies were specified with a code that was interpretable to IPA and based on the *Vsx2* and *Mitf* gene set classifications (available upon request). In cases when HX531 DEGs or DBZ DEGs were analyzed by ORA in the *mutants* dataset, gene lists were generated for these DEG sets (see below). ARMs and gene expression data were still pulled from the *mutants* dataset and were based on the *Vsx2* and *Mitf* gene set classification code.

Generation of NR and RPE gene lists—Bulk RNA sequencing data was obtained from Supplementary Table 1 in Andrabi et al⁹¹. We used the *Day15 +FGF / Day15 +Wnt* column under the header *Comparison of Gene Expression Levels* to identify NR genes. The inverse values for this column were generated and placed into a new column titled *Day15 +Wnt / Day15 +FGF*, which was then used to identify RPE genes. For each gene list, filtering was done to include only those genes with a gene expression ratio greater than 10 for each identity. This yielded 115 neural retina and 192 RPE genes. These lists were loaded into IPA for ORA with results reported in the *My Lists* section of the Core analysis output. The expression data from Andrabi and colleagues and the gene lists can be found in Suppl. File 7.

Generation of retinal cell type gene lists—Single-cell RNA-Seq data files were obtained from GEO accession: GSE118614⁵². The GSE118614_barcodes, GSE118614_genes, and GSE118614_10x_aggregate.mtx files were read into R and merged to generate a SC-RNA object which included the barcodes, genes, gene counts, and the relevant age and cell type metadata. The object then underwent filtering. Any cell with the ‘Doublets’ cell type and a cell age greater than E14.5 were filtered out of the object.

The FindMarkers function from the Seurat V3 package⁹² was used to identify differentially expressed genes between the cell types of interest and the remaining cell population in the object. The logfc.threshold was set to 0.10 and a Wilcoxon rank sum test was used to assess differential expression. The comparison groups to generate the resulting gene lists were:

1. ‘Neurogenic RPCs’ vs. all others
2. ‘Early RPCs’ vs. all others
3. ‘Amacrine Cells’ vs. all others
4. ‘Retinal Ganglion Cells’ vs. all others
5. ‘Cones’ and ‘Photoreceptor Precursors’ vs. all others
 - a. Cones and PhPrs were grouped into the same identity class.
6. ‘Horizontal Cells’ vs. all others
7. ‘RPE/Margin/Periocular Mesenchyme/Lens Epithelial Cells’ vs. all others

Filtering was done to restrict the number of differentially expressed genes to approximately 100 genes for each cell type. Filtering parameters included cutoffs for avg logFC, adj p-value and the ratio of the percentage of cells expressing each gene in the target cell type compared to all others (listed in Suppl. File 8). The resulting lists were then compared to identify shared genes, which were culled from all lists. *Ascl1* was the sole exception, which was assigned to the nRPC list based on its known function in RPCs. Culling negatively impacted the Amacrine (A) and Horizontal cell (HC) gene lists because of a dearth of cell type specific genes as well as a large overlap in shared genes between the two cell types. The gene lists were merged into a common A_HC gene list and the shared genes were retained. All gene lists were loaded into IPA and are provided in Suppl. File 9.

Generation of HX531 and DBZ DEG gene lists—All 67 HX531 DEGs were loaded into IPA with 53 retained for the HX531 gene list. All 376 DBZ DEGs were loaded into IPA with 375 retained for the DBZ gene list.

Quantitative reverse transcription PCR (qPCR)

Total RNA was isolated using TRIzol reagent (Thermo Fisher Scientific, Cat#15596026). cDNAs were synthesized using SuperScript IV VILO Master Mix (Thermo Fisher Scientific, Cat# 11766051). qPCR was done on QuantStudio 3 Real Time PCR Systems (Thermo Fisher Scientific) with the TaqMan gene expression Master Mix (Thermo Fisher Scientific, Cat# 444557) and TaqMan gene probes for *Abca1*, *Abcg1*, *Scd2*, *Gapdh* (Assay ID:

Abca1 - Mm00442646_m1; Abcg1 - Mm00437390_m1; Scd2 - Mm01028542_m1; Gapdh - Mm99999915_g1).

Relative changes in gene expression were determined with the delta-delta-Ct method (DDCt). Gapdh was used as the endogenous control for the initial normalization (DCt values). DDCt values were generated by normalizing DCt values to the mean DCt value of the control samples (untreated). Data is presented in graphs as the fold change in gene expression ($RQ = 2^{-DDCt}$). Graphing and statistical tests were done with GraphPad Prism (version 9.0) and Microsoft Excel (version 16.43). Descriptive statistics for RQ values and test results are provided in Supplemental File 2. Hypothesis testing was done on DDCt values.

Supplementary Material

Refer to Web version on PubMed Central for supplementary material.

Acknowledgements

We thank members of the Levine and Fuhrmann laboratories for their input over the course of this study, and Sabine Fuhrmann for reading the manuscript. We also thank Angela Jones at Vanderbilt Technologies for Advanced Genomics (VANTAGE) and Jean-Phillipe Cartailier at Creative Data Solutions for their assistance with RNA sequencing and data processing.

Funding was generously provided by the National Eye Institute (R01-EY013760, T32-EY021453, P30-EY008216) through an unrestricted grant from Research to Prevent Blindness, Inc. to the Department of Ophthalmology and Visual Sciences.

References

- Bürglin TR, Affolter M. Homeodomain proteins: an update. *Chromosoma*. 2016;125(3):497–521. 10.1007/s00412-015-0543-8 [PubMed: 26464018]
- Burmeister M, Novak J, Liang MY, et al. Ocular retardation mouse caused by Chx10 homeobox null allele: impaired retinal progenitor proliferation and bipolar cell differentiation. *Nature Genetics*. 1996;12(4):376–384. 10.1038/ng0496-376 [PubMed: 8630490]
- Reis LM, Khan A, Kariminejad A, Ebadi F, Tyler RC, Semina EV. VSX2 mutations in autosomal recessive microphthalmia. *Mol Vis*. 2011;17:2527–2532. [PubMed: 21976963]
- Truslove GM. A gene causing ocular retardation in the mouse. *J Embryol Exp Morph*. 1962;10:652–660. [PubMed: 13994395]
- Wright EM, Perveen R, Bowers N, et al. VSX2 in microphthalmia: a novel splice site mutation producing a severe microphthalmia phenotype. *British Journal of Ophthalmology*. 2010;94(3):386–388. 10.1136/bjo.2009.159996 [PubMed: 20215382]
- Zou C, Levine EM. Vsx2 Controls Eye Organogenesis and Retinal Progenitor Identity Via Homeodomain and Non-Homeodomain Residues Required for High Affinity DNA Binding. *Plos Genet*. 2012;8(9):e1002924. 10.1371/journal.pgen.1002924 [PubMed: 23028343]
- Liu ISC, de Chen J, Ploder L, et al. Developmental expression of a novel murine homeobox gene (Chx10): Evidence for roles in determination of the neuroretina and inner nuclear layer. *Neuron*. 1994;13(2):377–393. 10.1016/0896-6273(94)90354-9 [PubMed: 7914735]
- Horsford DJ, Nguyen MTT, Sellar GC, Kothary R, Arnheiter H, McInnes RR. Chx10 repression of Mitf is required for the maintenance of mammalian neuroretinal identity. *Development (Cambridge, England)*. 2005;132(1):177–187. 10.1242/dev.01571 [PubMed: 15576400]
- Green ES, Stubbs JL, Levine EM. Genetic rescue of cell number in a mouse model of microphthalmia: interactions between Chx10 and G1-phase cell cycle regulators. *Development*. 2003;130(3):539–552. 10.1242/dev.00275 [PubMed: 12490560]

10. Dhomen NS, Balaggan KS, Pearson RA, et al. Absence of *chx10* causes neural progenitors to persist in the adult retina. *Investigative ophthalmology & visual science*. 2006;47(1):386–396. 10.1167/iovs.05-0428 [PubMed: 16384989]
11. Bone-Larson C, Basu S, Radel JD, et al. Partial rescue of the ocular retardation phenotype by genetic modifiers. *J Neurobiol*. 2000;42(2):232–247. 10.1002/(sici)1097-4695(20000205)42:2<;aid-neu7>3.0.co;2-4 [PubMed: 10640330]
12. Sigulinsky CL, Green ES, Clark AM, Levine EM. *Vsx2/Chx10* ensures the correct timing and magnitude of Hedgehog signaling in the mouse retina. *Developmental biology*. 2008;317(2):560–575. 10.1016/j.ydbio.2008.02.055 [PubMed: 18417110]
13. Gago-Rodrigues I, Fernández-Miñán A, Letelier J, et al. Analysis of *opo* cis-regulatory landscape uncovers *Vsx2* requirement in early eye morphogenesis. *Nature communications*. 2015;6:7054. 10.1038/ncomms8054
14. Vitorino M, Jusuf PR, Maurus D, Kimura Y, Higashijima S ichi, Harris WA. *Vsx2* in the zebrafish retina: restricted lineages through derepression. *Neural Development*. 2009;4(1):14. 10.1186/1749-8104-4-14 [PubMed: 19344499]
15. Erclik T, Hartenstein V, Lipshitz HD, McInnes RR. Conserved Role of the *Vsx* Genes Supports a Monophyletic Origin for Bilaterian Visual Systems. *Curr Biol*. 2008;18(17):1278–1287. 10.1016/j.cub.2008.07.076 [PubMed: 18723351]
16. Altun-Gultekin Z, Andachi Y, Tsalik EL, Pilgrim D, Kohara Y, Hobert O. A regulatory cascade of three homeobox genes, *ceh-10*, *ttx-3* and *ceh-23*, controls cell fate specification of a defined interneuron class in *C. elegans*. *Development*. 2001;128(11):1951–1969. 10.1242/dev.128.11.1951 [PubMed: 11493519]
17. Rowan S, Chen CMAM, Young TL, Fisher DE, Cepko CL. Transdifferentiation of the retina into pigmented cells in ocular retardation mice defines a new function of the homeodomain gene *Chx10*. *Development (Cambridge, England)*. 2004;131(20). 10.1242/dev.01300
18. Bian F, Daghani M, Lu F, Liu S, Gross JM, Aldiri I. Functional analysis of *Vsx2* super-enhancer uncovers distinct cis-regulatory circuits controlling *Vsx2* expression during retinogenesis. *Development*. 2022;149(15). 10.1242/dev.200642
19. Capowski EE, Wright LS, Liang K, et al. Regulation of WNT Signaling by *VSX2* During Optic Vesicle Patterning in Human Induced Pluripotent Stem Cells. *STEM CELLS*. 2016;34(11):2625–2634. 10.1002/stem.2414 [PubMed: 27301076]
20. Sigulinsky CL, German ML, Leung AM, Clark AM, Yun S, Levine EM. Genetic chimeras reveal the autonomy requirements for *Vsx2* in embryonic retinal progenitor cells. *Neural Dev*. 2015;10(1):12. 10.1186/s13064-015-0039-5 [PubMed: 25927996]
21. Kindiakov BN, Koniukhov BV. [Mutant gene expression in murine aggregation chimeras. 5. The ocular retardation and fidget genes]. *Ontogenez*. 1986;17(1):47–55. [PubMed: 3960462]
22. Osipov VV, Vakhrusheva MP. [Clonal analysis of the development of the pigment epithelium of the eye in chimeric or/or---AKR mice]. *Ontogenez*. 1984;15(1):73–80. [PubMed: 6700941]
23. Katoh K, Omori Y, Onishi A, Sato S, Kondo M, Furukawa T. *Blimp1* suppresses *Chx10* expression in differentiating retinal photoreceptor precursors to ensure proper photoreceptor development. *J Neurosci Official J Soc Neurosci*. 2010;30(19):6515–6526. 10.1523/jneurosci.0771-10.2010
24. Brzezinski JA, Lamba DA, Reh TA. *Blimp1* controls photoreceptor versus bipolar cell fate choice during retinal development. *Development*. 2010;137(4):619–629. 10.1242/dev.043968 [PubMed: 20110327]
25. Gamm DM, Clark E, Capowski EE, Singh R. The Role of *Fgf9* In The Production of Neural Retina And Rpe In A Pluripotent Stem Cell Model of Early Human Retinal Development. *Am J Ophthalmol*. Published online 2019. 10.1016/j.ajo.2019.04.033
26. Nguyen MTT, Arnheiter H. Signaling and transcriptional regulation in early mammalian eye development: a link between FGF and *MITF*. *Development*. 2000;127(16):3581–3591. 10.1242/dev.127.16.3581 [PubMed: 10903182]
27. Kaufman ML, Park KU, Goodson NB, et al. Transcriptional profiling of murine retinas undergoing semi-synchronous cone photoreceptor differentiation. *Dev Biol*. 2019;453(2):155–167. 10.1016/j.ydbio.2019.05.016 [PubMed: 31163126]

28. Nelson BR, Hartman BH, Georgi SA, Lan MS, Reh TA. Transient inactivation of Notch signaling synchronizes differentiation of neural progenitor cells. *Dev Biol.* 2007;304(2):479–498. 10.1016/j.ydbio.2007.01.001 [PubMed: 17280659]
29. Lehner B Molecular mechanisms of epistasis within and between genes. *Trends Genet.* 2011;27(8):323–331. 10.1016/j.tig.2011.05.007 [PubMed: 21684621]
30. Fuhrmann S Chapter Three Eye Morphogenesis and Patterning of the Optic Vesicle. *Curr Top Dev Biol.* 2010;93:61–84. 10.1016/b978-0-12-385044-7.00003-5 [PubMed: 20959163]
31. Westenskow P, Piccolo S, Fuhrmann S. β -catenin controls differentiation of the retinal pigment epithelium in the mouse optic cup by regulating *Mitf* and *Otx2* expression. *Development.* 2009;136(15):2505–2510. 10.1242/dev.032136 [PubMed: 19553286]
32. Bharti K, Nguyen MT, Skuntz S, Bertuzzi S, Arnheiter H. The other pigment cell: specification and development of the pigmented epithelium of the vertebrate eye. *Pigment Cell Research.* 2006;19(5):380–394. 10.1111/j.1600-0749.2006.00318.x [PubMed: 16965267]
33. Chow RL, Lang RA. Early eye development in vertebrates. *Annual review of cell and developmental biology.* 2001;17:255–296. 10.1146/annurev.cellbio.17.1.255
34. Bora N, Conway SJ, Liang H, Smith SB. Transient overexpression of the *Microphthalmia* gene in the eyes of *Microphthalmia vitiligo* mutant mice. *Dev Dynam.* 1998;213(3):283–292. 10.1002/(sici)1097-0177(199811)213:3<<
35. Yun S, Saijoh Y, Hirokawa KE, et al. *Lhx2* links the intrinsic and extrinsic factors that control optic cup formation. *Development.* 2009;136(23):3895–3906. 10.1242/dev.041202 [PubMed: 19906857]
36. Arnheiter H, Hou L, Nguyen MTT, et al. From Melanocytes to Melanoma, The Progression to Malignancy. *springer.* Published online 2006:27–49. 10.1007/978-1-59259-994-3_2
37. Konyukhov B, Sazhina M. Interaction of the genes of ocular retardation and microphthalmia in mice. *Folia biologica.* 1966;12(2):116–123. [PubMed: 4958088]
38. Bharti K, Liu W, Csermely T, Bertuzzi S, Arnheiter H. Alternative promoter use in eye development: the complex role and regulation of the transcription factor *MITF*. *Development.* 2008;135(6):1169–1178. 10.1242/dev.014142 [PubMed: 18272592]
39. Sharma RK, Netland PA. Early born lineage of retinal neurons express class III β -tubulin isotype. *Brain Res.* 2007;1176:11–17. 10.1016/j.brainres.2007.07.090 [PubMed: 17900541]
40. Pacal M, Bremner R. Induction of the ganglion cell differentiation program in human retinal progenitors before cell cycle exit. *Dev Dynam.* 2014;243(5):712–729. 10.1002/dvdy.24103
41. Barton KM, Levine EM. Expression patterns and cell cycle profiles of PCNA, MCM6, cyclin D1, cyclin A2, cyclin B1, and phosphorylated histone H3 in the developing mouse retina. *Developmental dynamics : an official publication of the American Association of Anatomists.* 2008;237(3):672–682. 10.1002/dvdy.21449 [PubMed: 18265020]
42. Hodgkinson CA, Moore KJ, Nakayama A, et al. Mutations at the mouse microphthalmia locus are associated with defects in a gene encoding a novel basic-helix-loop-helix-zipper protein. *Cell.* 1993;74(2):395–404. 10.1016/0092-8674(93)90429-t [PubMed: 8343963]
43. Hemesath T, Steingrímsson E, McGill G, et al. microphthalmia, a critical factor in melanocyte development, defines a discrete transcription factor family. *Genes & Development.* 1994;8(22):2770–2780. 10.1101/gad.8.22.2770 [PubMed: 7958932]
44. Steingrímsson E, Moore KJ, Lamoreux ML, et al. Molecular basis of mouse microphthalmia (*mi*) mutations helps explain their developmental and phenotypic consequences. *Nature genetics.* 1994;8(3):256–263. 10.1038/ng1194-256 [PubMed: 7874168]
45. Steingrímsson E, Arnheiter H, Hallsson JH, Lamoreux ML, Copeland NG, Jenkins NA. Interallelic Complementation at the Mouse *Mitf* Locus. *Genetics.* 2003;163(1):267–276. 10.1093/genetics/163.1.267 [PubMed: 12586714]
46. Slavi N, Balasubramanian R, Lee MA, et al. CyclinD2-mediated regulation of neurogenic output from the retinal ciliary margin is perturbed in albinism. *Neuron.* 2023;111(1):49–64.e5. 10.1016/j.neuron.2022.10.025 [PubMed: 36351424]
47. Jin K, Xiang M. Transitional Progenitors during Vertebrate Retinogenesis. *Mol Neurobiol.* 2017;54(5):3565–3576. 10.1007/s12035-016-9899-x [PubMed: 27194297]

48. Shiao F, Ruzycski PA, Clark BS. A single-cell guide to retinal development: Cell fate decisions of multipotent retinal progenitors in scRNA-seq. *Dev Biol.* 2021;478:41–58. 10.1016/j.ydbio.2021.06.005 [PubMed: 34146533]
49. Krämer A, Green J, Pollard J, Tugendreich S. Causal analysis approaches in Ingenuity Pathway Analysis. *Bioinformatics.* 2014;30(4):523–530. 10.1093/bioinformatics/btt703 [PubMed: 24336805]
50. Chen H, Lukas TJ, Du N, Suyeoka G, Neufeld AH. Dysfunction of the Retinal Pigment Epithelium with Age: Increased Iron Decreases Phagocytosis and Lysosomal Activity. *Investigative Ophthalmology Vis Sci.* 2009;50(4):1895. 10.1167/iops.08-2850
51. Wavre-Shapton ST, Meschede IP, Seabra MC, Futter CE. Phagosome maturation during endosome interaction revealed by partial rhodopsin processing in retinal pigment epithelium. *J Cell Sci.* 2014;127(17):3852–3861. 10.1242/jcs.154757 [PubMed: 25074813]
52. Clark BS, Stein-O'Brien GL, Shiao F, et al. Single-Cell RNA-Seq Analysis of Retinal Development Identifies NFI Factors as Regulating Mitotic Exit and Late-Born Cell Specification. *Neuron.* 2019;102(6):1111–1126.e5. 10.1016/j.neuron.2019.04.010 [PubMed: 31128945]
53. Cvekl A, Wang WL. Retinoic acid signaling in mammalian eye development. *Experimental Eye Research.* 2009;89(3):280–291. 10.1016/j.exer.2009.04.012 [PubMed: 19427305]
54. Hoover F, Seleiro EA, Kielland A, Brickell PM, Glover JC. Retinoid X receptor gamma gene transcripts are expressed by a subset of early generated retinal cells and eventually restricted to photoreceptors. *J Comp Neurology.* 1998;391(2):204–213.
55. Roberts MR, Hendrickson A, McGuire CR, Reh TA. Retinoid X Receptor γ Is Necessary to Establish the S-opsin Gradient in Cone Photoreceptors of the Developing Mouse Retina. *Investigative Ophthalmology Vis Sci.* 2005;46(8):2897. 10.1167/iops.05-0093
56. Buenaventura DF, Corseri A, Emerson MM. Identification of Genes With Enriched Expression in Early Developing Mouse Cone Photoreceptors. *Invest Ophth Vis Sci.* 2019;60(8):2787–2799. 10.1167/iops.19-26951
57. Lyu J, Mu X. Genetic control of retinal ganglion cell genesis. *Cell Mol Life Sci.* 2021;78(9):4417–4433. 10.1007/s00018-021-03814-w [PubMed: 33782712]
58. Mori M, Ghyselinck NB, Chambon P, Mark M. Systematic immunolocalization of retinoid receptors in developing and adult mouse eyes. *Invest Ophth Vis Sci.* 2001;42(6):1312–1318.
59. Nie B, Nie T, Hui X, et al. Brown Adipogenic Reprogramming Induced by a Small Molecule. *Cell Reports.* 2017;18(3):624–635. 10.1016/j.celrep.2016.12.062 [PubMed: 28099842]
60. Sun Y, Hao M, Luo Y, et al. Stearoyl-CoA Desaturase Inhibits ATP-binding Cassette Transporter A1-mediated Cholesterol Efflux and Modulates Membrane Domain Structure*. *J Biol Chem.* 2003;278(8):5813–5820. 10.1074/jbc.m208687200 [PubMed: 12482877]
61. Matsuo M ABCA1 and ABCG1 as potential therapeutic targets for the prevention of atherosclerosis. *J Pharmacol Sci.* 2022;148(2):197–203. 10.1016/j.jphs.2021.11.005 [PubMed: 35063134]
62. Kastner P, Grondona JM, Mark M, et al. Genetic analysis of RXR α developmental function: Convergence of RXR and RAR signaling pathways in heart and eye morphogenesis. *Cell.* 1994;78(6):987–1003. 10.1016/0092-8674(94)90274-7 [PubMed: 7923367]
63. Kastner P, Mark M, Ghyselinck N, et al. Genetic evidence that the retinoid signal is transduced by heterodimeric RXR/RAR functional units during mouse development. *Dev Camb Engl.* 1997;124(2):313–326. 10.1242/dev.124.2.313
64. Visel A, Thaller C, Eichele G. GenePaint.org: an atlas of gene expression patterns in the mouse embryo. *Nucleic Acids Res.* 2004;32(suppl_1):D552–D556. 10.1093/nar/gkh029 [PubMed: 14681479]
65. Mills EA, Goldman D. The Regulation of Notch Signaling in Retinal Development and Regeneration. *Current Pathobiology Reports.* 2017;5(4):323–331. 10.1007/s40139-017-0153-7 [PubMed: 29354328]
66. Jadhav AP, Cho SHH, Cepko CL. Notch activity permits retinal cells to progress through multiple progenitor states and acquire a stem cell property. *Proceedings of the National Academy of Sciences of the United States of America.* 2006;103(50):18998–19003. 10.1073/pnas.0608155103 [PubMed: 17148603]

67. Perron M, Harris WA. Determination of vertebrate retinal progenitor cell fate by the Notch pathway and basic helix-loop-helix transcription factors. *Cell Mol Life Sci Cmls*. 2000;57(2):215–223. 10.1007/pl00000685 [PubMed: 10766018]
68. Dorsky RI, Rapaport DH, Harris WA. Xotch inhibits cell differentiation in the *Xenopus* retina. *Neuron*. 1995;14(3):487–496. [PubMed: 7695895]
69. Jadhav AP, Mason HA, Cepko CL. Notch 1 inhibits photoreceptor production in the developing mammalian retina. *Development (Cambridge, England)*. 2006;133(5):913–923. 10.1242/dev.02245 [PubMed: 16452096]
70. Riesenberger AN, Liu Z, Kopan R, Brown NL. Rbpj cell autonomous regulation of retinal ganglion cell and cone photoreceptor fates in the mouse retina. *J Neurosci*. 2009;29(41):12865–12877. 10.1523/jneurosci.3382-09.2009 [PubMed: 19828801]
71. Zheng MH, Shi M, Pei Z, Gao F, Han H, Ding YQ. The transcription factor RBP-J is essential for retinal cell differentiation and lamination. *Mol Brain*. 2009;2(1):38. 10.1186/1756-6606-2-38 [PubMed: 20017954]
72. Strooper BD, Annaert W, Cupers P, et al. A presenilin-1-dependent γ -secretase-like protease mediates release of Notch intracellular domain. *Nature*. 1999;398(6727):518–522. 10.1038/19083 [PubMed: 10206645]
73. Olsauskas-Kuprys R, Zlobin A, Osipo C. Gamma secretase inhibitors of Notch signaling. *Oncotargets Ther*. 2013;6:943–955. 10.2147/ott.s33766
74. Güner G, Lichtenthaler SF. The substrate repertoire of γ -secretase/presenilin. *Semin Cell Dev Biol*. 2020;105:27–42. 10.1016/j.semcdb.2020.05.019 [PubMed: 32616437]
75. Luo H, Jin K, Xie Z, et al. Forkhead box N4 (Foxn4) activates Dll4-Notch signaling to suppress photoreceptor cell fates of early retinal progenitors. *Proceedings of the National Academy of Sciences of the United States of America*. 2012;109(9):E553–62. 10.1073/pnas.1115767109 [PubMed: 22323600]
76. García-Llorca A, Aspelund SG, Ogmundsdottir MH, Steingrímsson E, Eysteinnsson T. The microphthalmia-associated transcription factor (Mitf) gene and its role in regulating eye function. *Sci Rep-uk*. 2019;9(1):15386. 10.1038/s41598-019-51819-0
77. Wen B, Li S, Li H, et al. Microphthalmia-associated transcription factor regulates the visual cycle genes *Rbp1* and *Rdh5* in the retinal pigment epithelium. *Sci Rep-uk*. 2016;6(1):21208. 10.1038/srep21208
78. Bumsted K, Barnstable C. Dorsal retinal pigment epithelium differentiates as neural retina in the microphthalmia (mi/mi) mouse. *Investigative ophthalmology & visual science*. 2000;41(3):903–908. [PubMed: 10711712]
79. Storti F, Klee K, Todorova V, et al. Impaired ABCA1/ABCG1-mediated lipid efflux in the mouse retinal pigment epithelium (RPE) leads to retinal degeneration. *Elife*. 2019;8:e45100. 10.7554/elife.45100 [PubMed: 30864945]
80. Frambach SJCM, de Haas R, Smeitink JAM, Rongen GA, Russel FGM, Schirris TJJ. Brothers in Arms: ABCA1- and ABCG1-Mediated Cholesterol Efflux as Promising Targets in Cardiovascular Disease Treatment. *Pharmacol Rev*. 2020;72(1):152–190. 10.1124/pr.119.017897 [PubMed: 31831519]
81. McCaffery P, Posch KC, Napoli JL, Gudas L, Dräger UC. Changing Patterns of the Retinoic Acid System in the Developing Retina. *Dev Biol*. 1993;158(2):390–399. 10.1006/dbio.1993.1197 [PubMed: 8393814]
82. Duester G Towards a Better Vision of Retinoic Acid Signaling during Eye Development. *Cells*. 2022;11(3):322. 10.3390/cells11030322 [PubMed: 35159132]
83. Thompson B, Katsanis N, Apostolopoulos N, Thompson DC, Nebert DW, Vasiliou V. Genetics and functions of the retinoic acid pathway, with special emphasis on the eye. *Hum Genomics*. 2019;13(1):61. 10.1186/s40246-019-0248-9 [PubMed: 31796115]
84. Chew SH, Martinez C, Chirco KR, Kandoi S, Lamba DA. Timed Notch Inhibition Drives Photoreceptor Fate Specification in Human Retinal Organoids. *Invest Ophth Vis Sci*. 2022;63(10):12. 10.1167/iovs.63.10.12
85. Levine EM, Green ES. Cell-intrinsic regulators of proliferation in vertebrate retinal progenitors. *Semin Cell Dev Biol*. 2004;15(1):63–74. 10.1016/j.semcdb.2003.09.001 [PubMed: 15036209]

86. Wanek N, Muneoka K, Holler-dinsmore G, Burton R, Bryant S. A staging system for mouse limb development. *Journal of Experimental Zoology*. 1989;249(1):41–49. 10.1002/jez.1402490109 [PubMed: 2926360]
87. Schindelin J, Arganda-Carreras I, Frise E, et al. Fiji: an open-source platform for biological-image analysis. *Nat Methods*. 2012;9(7):676–682. 10.1038/nmeth.2019 [PubMed: 22743772]
88. Dobin A, Davis CA, Schlesinger F, et al. STAR: ultrafast universal RNA-seq aligner. *Bioinformatics*. 2013;29(1):15–21. 10.1093/bioinformatics/bts635 [PubMed: 23104886]
89. Anders S, Pyl PT, Huber W. HTSeq—a Python framework to work with high-throughput sequencing data. *Bioinformatics*. 2015;31(2):166–169. 10.1093/bioinformatics/btu638 [PubMed: 25260700]
90. Love MI, Huber W, Anders S. Moderated estimation of fold change and dispersion for RNA-seq data with DESeq2. *Genome Biol*. 2014;15(12):550. 10.1186/s13059-014-0550-8 [PubMed: 25516281]
91. Andrabi M, Kuraku S, Takata N, Sasai Y, Love NR. Comparative, transcriptome analysis of self-organizing optic tissues. *Sci Data*. 2015;2(1):150030. 10.1038/sdata.2015.30 [PubMed: 26110066]
92. Stuart T, Butler A, Hoffman P, et al. Comprehensive Integration of Single-Cell Data. *Cell*. 2019;177(7):1888–1902.e21. 10.1016/j.cell.2019.05.031 [PubMed: 31178118]

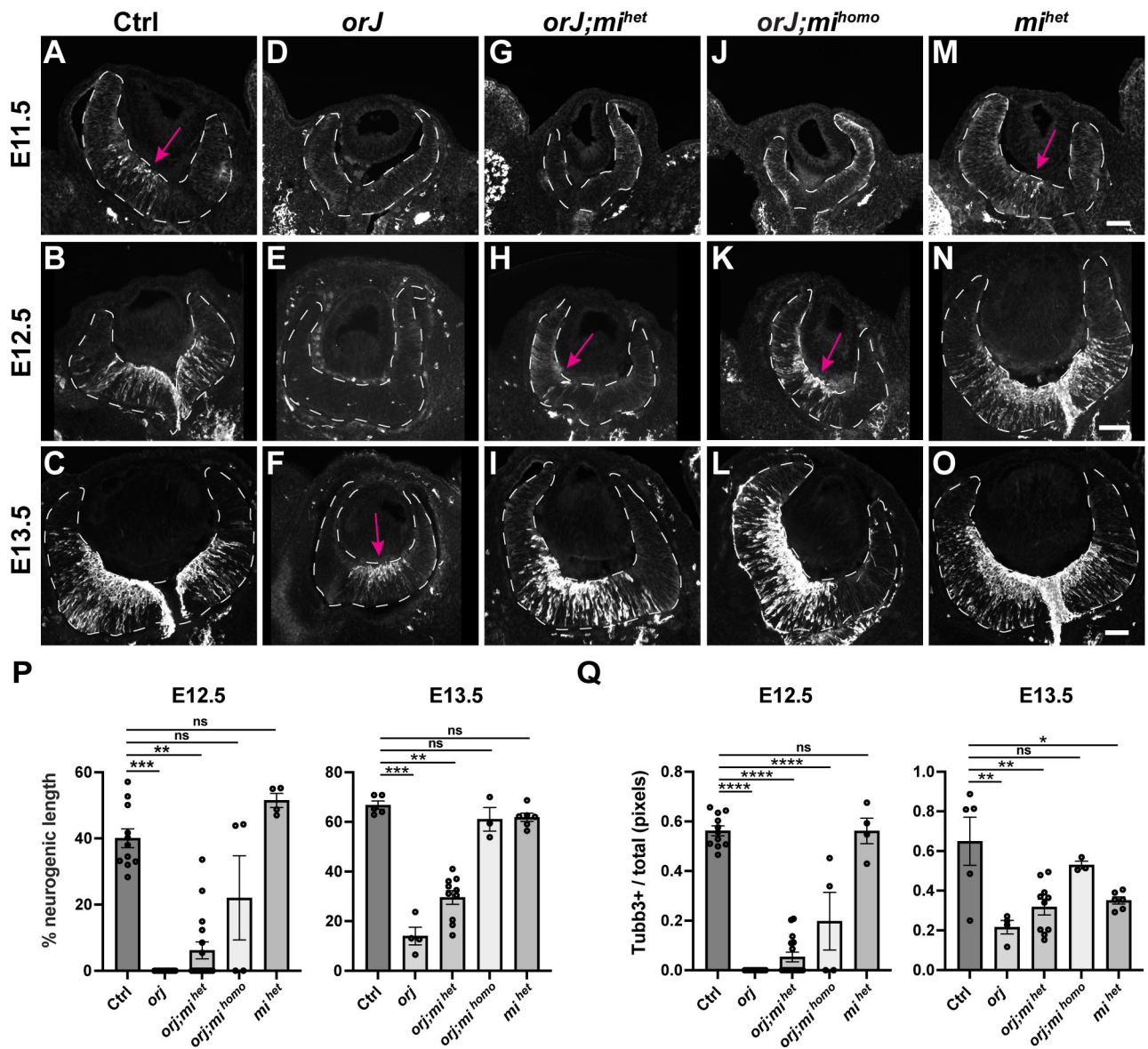


Figure 1: *Mitf* contributes to the delayed onset of neurogenesis in the *orJ* retina.

(A-O) Tubb3 staining marks post-mitotic neuronal precursors from E11.5 – E13.5. Retinas are within dashed lines; magenta arrows point out the initial appearance of Tubb3 in each genotype. Scale bars: 50 μ M (by age). **(A-C)** Tubb3+ cells are evident in the *orJ^{het}* (control) retina at E11.5, extending across the retina at E12.5 and E13.5. **(D-F)** In the *orJ* retina, Tubb3+ cells do not appear until E13.5. **(G-I)** Tubb3+ cells are detected in the *orJ; mi^{het}* retina at E12.5, with enhanced accumulation at E13.5. **(J-L)** Tubb3 expression is not observed at E11.5 in the *orJ; mi^{homo}* retina but is detected at E12.5. **(M-O)** Tubb3+ cells are observed at all three ages in the *mi^{het}* retina. **(P)** Quantification of Tubb3 expression across the retina as a percentage of retinal length (neurogenic progression) at E12.5 and E13.5. **(Q)** Quantification of Tubb3+ pixels as a fraction of the total pixels within neurogenic regions was used as a measure of neurogenic output at E12.5 and E13.5.

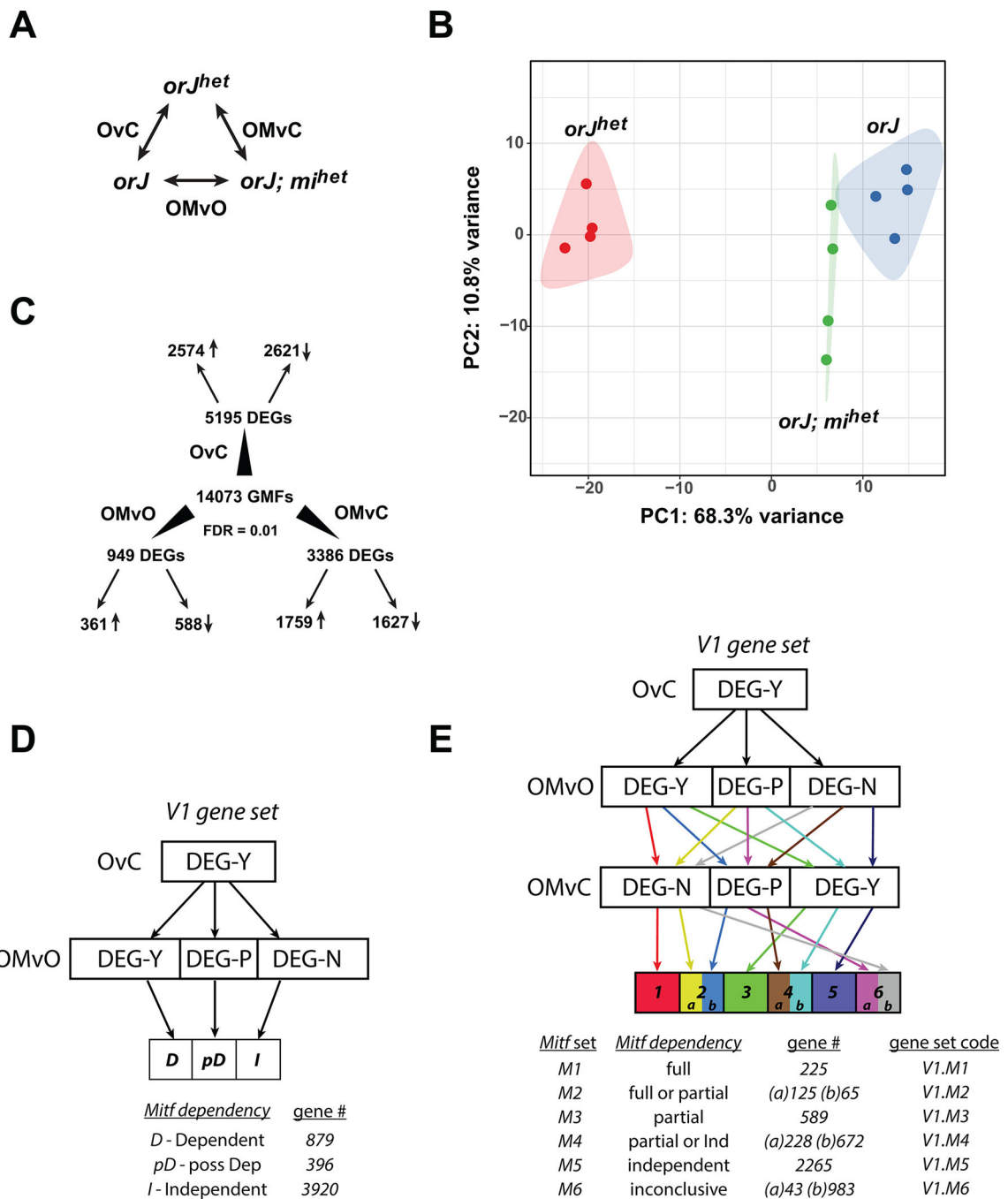


Figure 2: The *mi* mutation partially restores gene expression in the E12.5 *orJ* retina.
 (A) Tripartite design of differential gene expression analysis of RNA sequencing data across the 3 genotypes. Comparisons were made between *or^Jhet* (C - control), *or^Jhomo* (O) and *or^Jhomo; mi^Jhet* (OM) with 4 biological replicates per genotype. Genotype in first position was compared against the genotype in the second position for each comparison, thereby assigning the directions of expression changes to the first genotype. (B) PCA plot for the transcriptomes from each replicate. (C) Summary of differential expression analysis between the 3 genotypes. Genes were assigned as DEGs if they were within the 0.01 FDR cutoff.

DEGs were then split by their directional change in expression (small arrows). **(D)** DEG status of the V1 genes (see Table 1) in the OMvO comparison identified three categories of *Mitf* dependency. **(E)** Gene set classification of the *Vsx2*-dependent genes (V1 gene set) based on *Mitf*-dependence as determined from the OMvO and OMvC comparisons yielded 6 gene sets (see text for details). Suppl. File 4 provides similar classifications for the *Vsx2*-possibly dependent (V2) and *Vsx2*-independent (V3) genes (see Table 1).

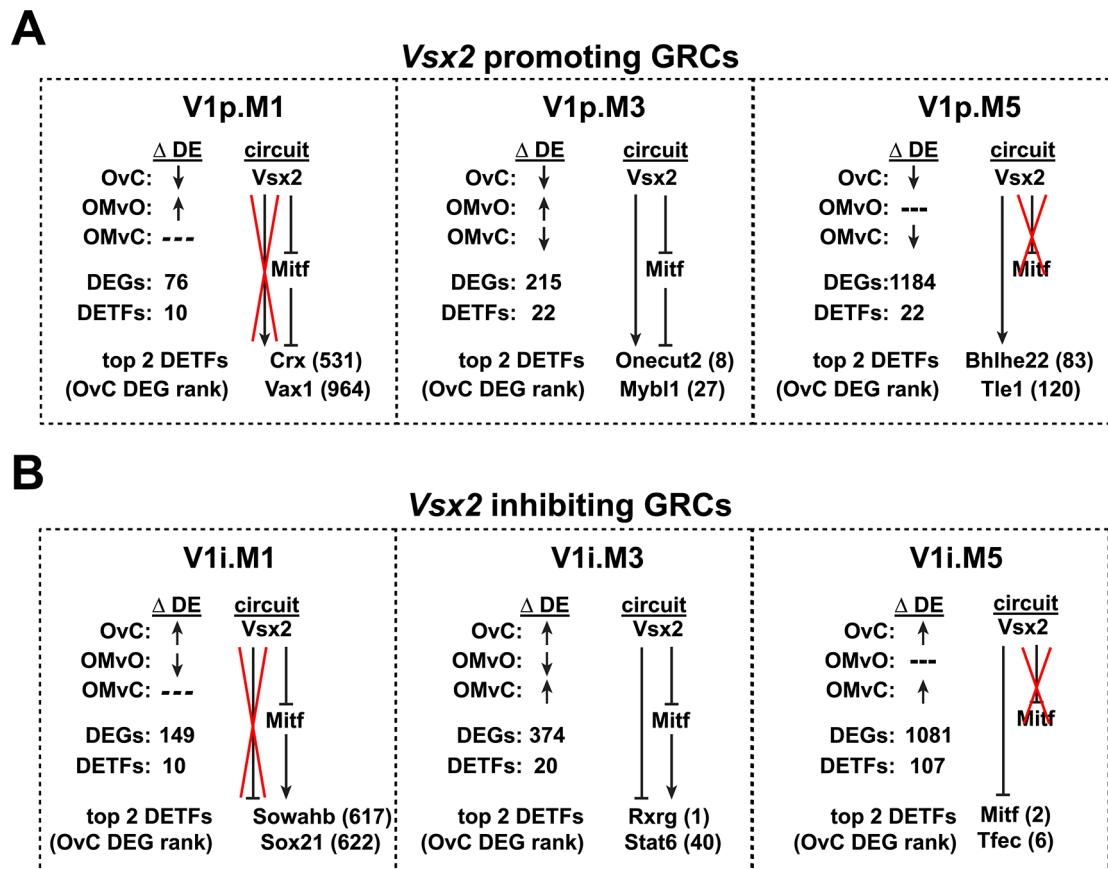


Figure 3: Classification of V1 genes into gene regulatory circuits (GRCs) based on *Mitf*-dependency and directional changes in gene expression.

V1.M1, V1.M3, and V1.M5 genes were split into GRCs based on their predicted regulation by *Vsx2* and *Mitf*. (A) Genes that are promoted by *Vsx2* were designated as V1p. (B) Genes that are inhibited by *Vsx2* were designated as V1i. The red X denotes branches that are not employed in the respective GRC. The number of DEGs and differentially expressed transcription factors (DETFs) are provided for each GRC and the top 2 DETFs by DEG rank (adj-p from OvC comparison) are shown.

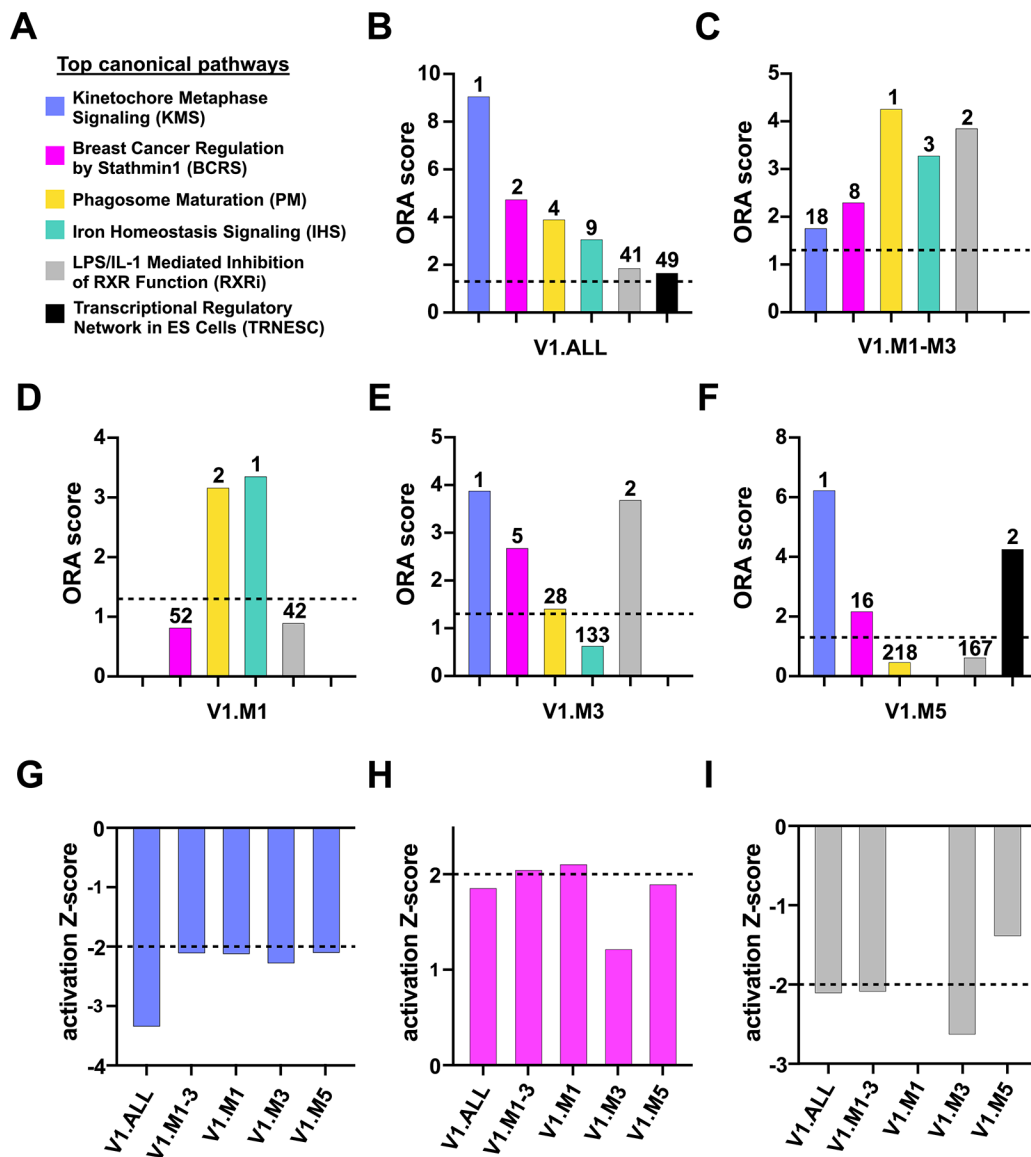


Figure 4: Comparison of overrepresented canonical pathways in V1 gene sets. CP-ORA was done for the full cohort of V1 genes (V1.ALL), for *Mitf*-dependent genes (V1.M1-M3; V1.M1; V1.M3) and *Mitf*-independent genes (V1.M5). (A) The two top ranked pathways for each gene set based on ORA score are indicated. 6 canonical pathways were identified across the 5 gene sets. (B-F) Distribution of the 6 pathways by ORA score (y-axis) and rank (numbers above bars) for the V1.ALL, V1.M1-M3, V1.M1, V1.M3, and V1.M5 gene sets. ORA scores > 1.3 are considered significant. (G-I) Activation Z-scores for the KMS, BCRS, and RXRi pathways for each gene set. Positive scores predict pathway activation; negative scores predict inhibition. Dashed lines indicate thresholds for significance.

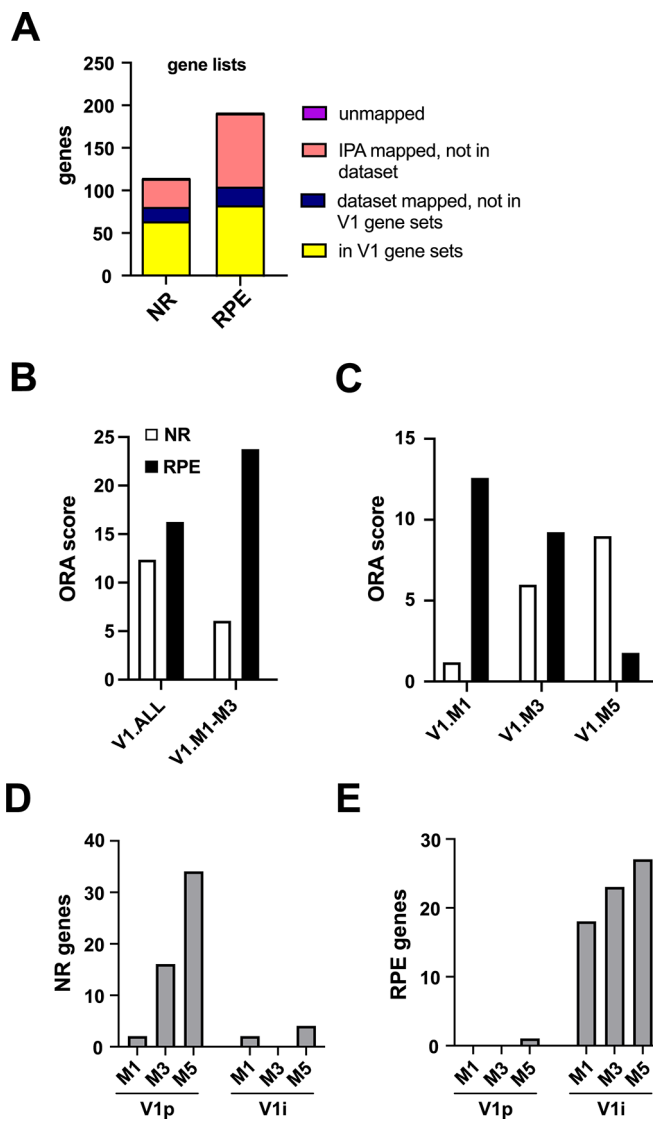


Figure 5: *Mitf* differentially impacts the expression of V1 genes associated with neural retina (NR) and RPE identities.

ORA using differentially expressed genes culled from published RNA sequencing data of FGF- or Wnt-treated ESC-derived optic cup organoids to promote neural retina (NR) or RPE identities, respectively (Andrabe et al., 2015). **(A)** Distribution of genes in each list. Dataset mapped genes (blue and yellow bars) were used for ORA analysis. **(B)** ORA scores for the NR gene list (white bars) and RPE gene list (black bars) in the V1.ALL and V1.M1-M3 gene sets. **(C)** ORA scores for the NR and RPE gene lists in the V1.M1, V1.M3, and V1.M5 gene sets. **(D)** Distribution of genes from the NR gene list by GRC. **(E)** Distribution of genes from the RPE gene list by GRC.

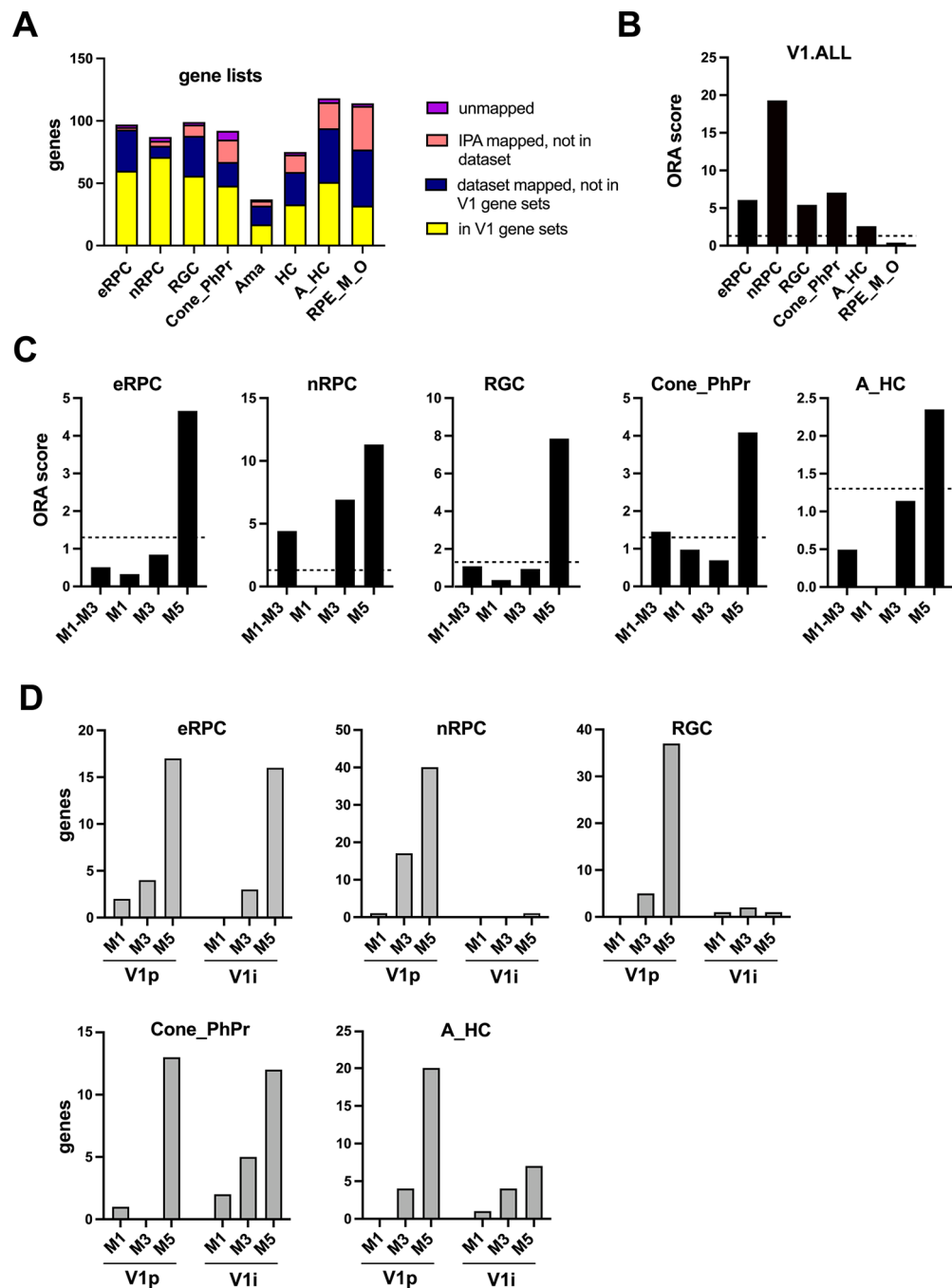


Figure 6: *Mitf* has a modest impact on the expression of V1 genes associated with retinal neurogenesis.

ORA using gene lists representing retinal cell types from published scRNA-seq data of E11.5, E12.5, and E14.5 mouse retinas (Clarke, et al., 2019). (A) Distribution of genes in each cell type list. Dataset mapped genes (blue and yellow bars) were used for ORA analysis. The cone and photoreceptor precursor (PhPr) gene lists were combined (Cone_PhPr) because of high gene overlap and low numbers of dataset mapped genes as separate lists. The same was done for amacrine (Ama) and horizontal cells (HC). RPE_M_O

is not a true cell type but was assigned as a cell label in Clarke et al. (2019). **(B)** ORA scores for the cell type gene lists in the V1.ALL gene set. **(C)** ORA scores for each cell type gene lists from the V1.M1-M3, V1.M1, V1.M3, and V1.M5 gene sets. The RPE_M_O gene list was not included because of its low ORA score in the V1.ALL gene set. Dashed lines indicate significance threshold of 1.3, which is equivalent to a p-value of 0.05. **(D)** Distribution of genes from the cell type gene lists by GRC.

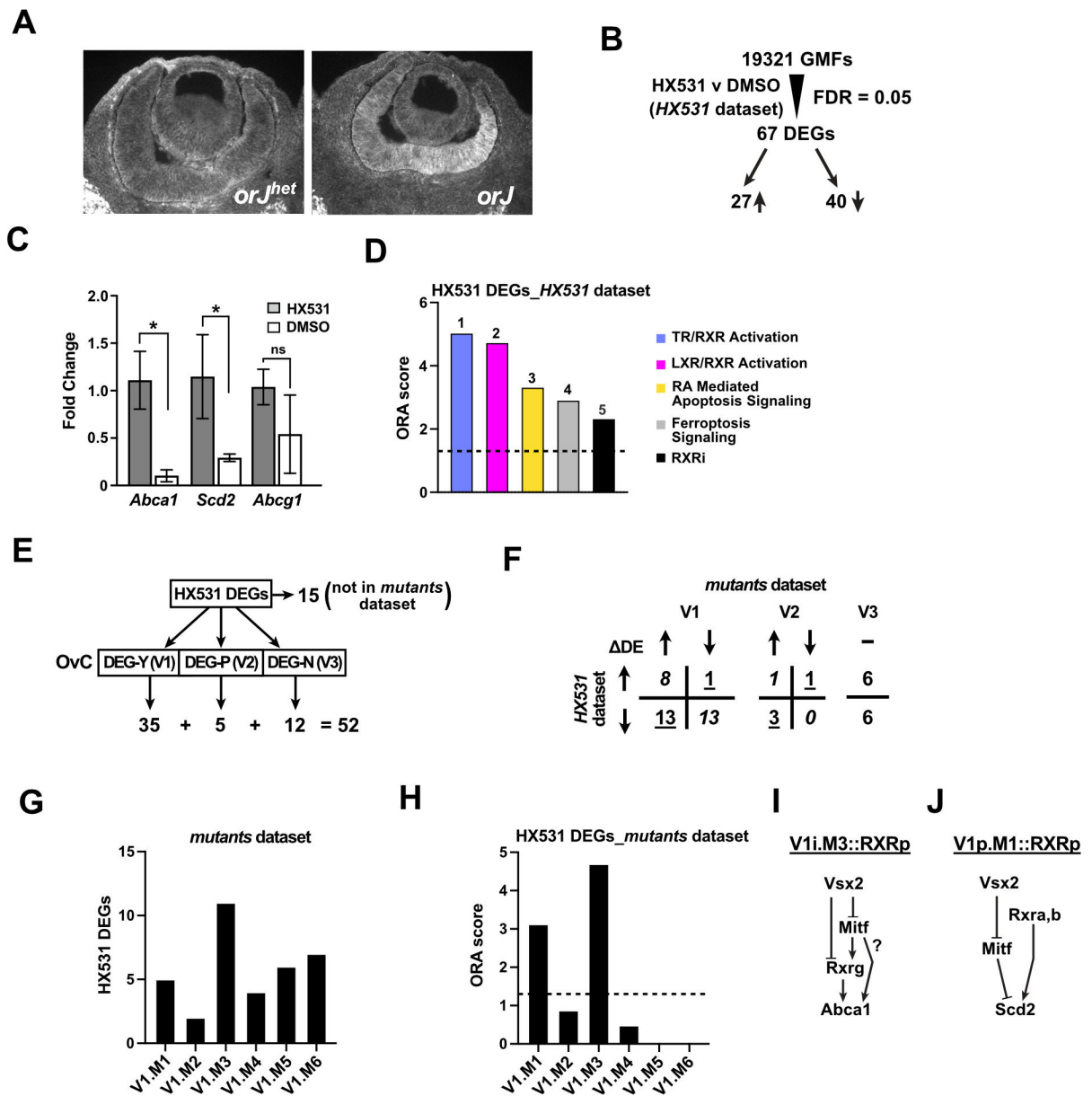


Figure 7: *Rrxg* is upregulated in the *orJ* retina but inhibition of RXR activity with HX531 has a small but measurable effect on gene expression.

(A) Immunohistochemistry for *Rrxg* expression in the E12.5 *orJ^{het}* (control; left panel) and *orJ* retina (right panel). (B) Bulk RNA sequencing of E12.5 *orJ* retinal tissues following HX531 treatment for 24 hr in explant culture. Pairwise comparison of the gene expression profiles from the HX531-treated and vehicle-treated (0.1% DMSO) samples identified 67 DEGs from 19321 GMFs when an FDR cutoff of 0.05 was applied. Of these, 27 were upregulated and 40 downregulated by HX531 treatment. (C) Consistent with the RNA seq data, qPCR of *Abca1* and *Scd2* shows reduced expression due to HX531 treatment. The effect on *Abcg1* expression was not statistically significant. (D) CP-ORA of the HX531 DEGs in the *HX531* dataset identified multiple pathways associated with RXR function. The numbers over each bar indicate their rank based on the ORA score. (E) ORA scores for the same pathways

from the CP-ORA analysis of the V1.ALL genes in the *mutants* dataset. Only two pathways were significantly overrepresented and their ranks by ORA score are indicated. **(F)** Filtering of the 67 DEGs through the *mutants* dataset identified 52 DEGs with different degrees of *Vsx2*-dependence. 15 HX531 DEGs were not identified in the *mutants* data. **(G)** Distribution of the 52 HX531 DEGs by their directional changes in expression (DE) in the *HX531* dataset (rows) and the *mutants* dataset separated by *Vsx2*-dependencies (columns). **(H)** Distribution of HX531 DEGs in the V1 gene set by *Mitf*-dependency. **(I)** ORA analysis of the HX531 DEGs in the *mutants* data. **(J)** Predicted GRC for *Abca1*. Whether the regulatory impact of *Mitf* on *Abca1* expression is mediated by *Rxrg* alone is an open question. **(K)** Predicted GRC for *Scd2*. Whereas *Mitf* accounts for increased *Scd2* expression in the *orJ* retina, HX531 treatment suggests RXR activity through *Rxra* or *Rxrb* could be promoting *Scd2* expression in the wild type retina.

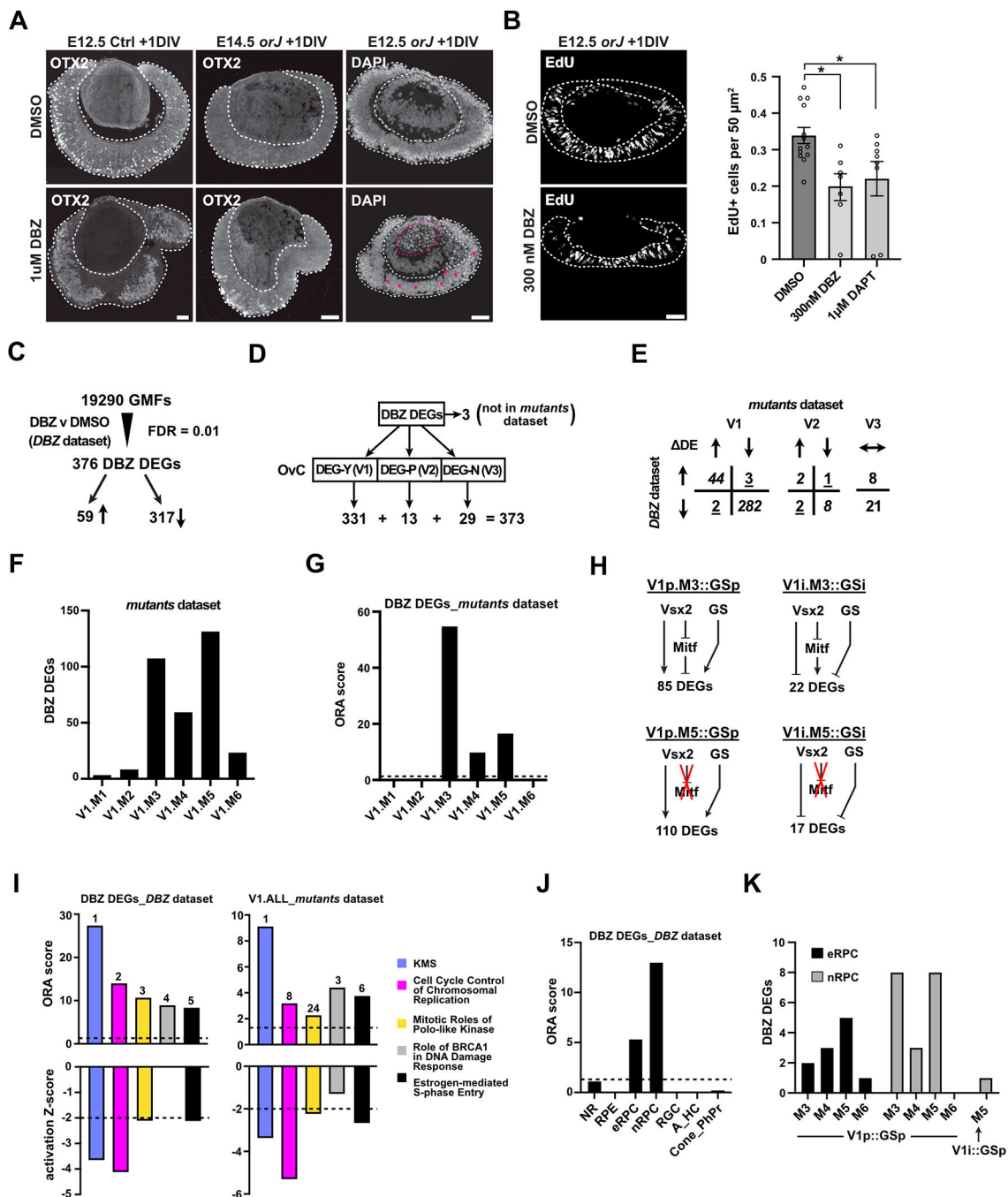


Figure 8: gamma-Secretase (GS) inhibition has a negative impact on the expression of *Vsx2*-dependent genes in the *orJ* retina.

(A, B) E12.5 retinal explants were cultured for 24 hr (1DIV). Retinal tissue is contained within the dashed lines. Scale bars: 50 μm. (A) *Otx2* expression and DAPI staining in retinal explants cultured in vehicle (0.1% DMSO) or 1μM DBZ. Left column shows E12.5 *orJ^{het}* (Ctrl) retinas, middle column shows E14.5 *orJ* retinas, and right column shows E12.5 *orJ* retinas. Examples of pyknotic nuclei are shown with DAPI staining in the retina (arrows) and in the lens (purple dashed line). (B) EdU incorporation in E12.5 *orJ* retinal explants

cultured in vehicle or 300 nM DBZ. Quantification of EdU+ cells. Error bars show S.E.M. Adjusted p-values were calculated with Tukey's multiple comparisons test following 1-way ANOVA. **(C)** Summary of RNA sequencing and differential gene expression from DBZ- and vehicle-treated E12.5 *orJ* explants. FDR cutoff of 0.01 was used to identify DEGs (376 DBZ DEGs). Up and down arrows indicate increased or decreased expression, respectively, in the DBZ-treated *orJ* retina. **(D)** Filtering of the 376 DEGs through the *mutants* dataset identified 373 DEGs with different degrees of *Vsx2*-dependence. 3 DBZ DEGs were not identified in the *mutants* data. **(E)** Distribution of the 373 DBZ DEGs by their directional changes in expression (DE) in the *DBZ* dataset (rows) and in the *mutants* dataset separated by *Vsx2*-dependencies (columns). **(F)** Distribution of DBZ DEGs in the V1 gene sets. **(G)** ORA analysis of the DBZ DEGs within the V1 gene sets in the *mutants* dataset. **(H)** GRCs that contain the highest numbers of DBZ DEGs in the V1.M3 and V1.M5 gene sets. Genes promoted by GS activity are referred to as GSp; inhibited genes are referred to as GSi. **(I)** The top 5 pathways identified by CP-ORA analysis of the DBZ DEGs in the *DBZ* dataset (upper left graph). The lower left graph shows the activation Z-scores for the 5 pathways. Negative Z-scores predict pathway inhibition. Significance thresholds are indicated with dashed lines. The upper right graph shows the same pathways as they were identified by CP-ORA for *Vsx2*-dependent genes (V1.ALL) in the *mutants* dataset with their rank by ORA score indicated above the bars. The lower right graph shows activation Z-scores for the pathways. **(J)** ORA analysis of the DBZ DEGs in the *DBZ* dataset with respect to the cell type gene lists. Dashed line indicates the threshold for significance. **(K)** Distribution of DBZ DEGs in the eRPC and nRPC genes lists by *Mitf*-dependence and GRC.

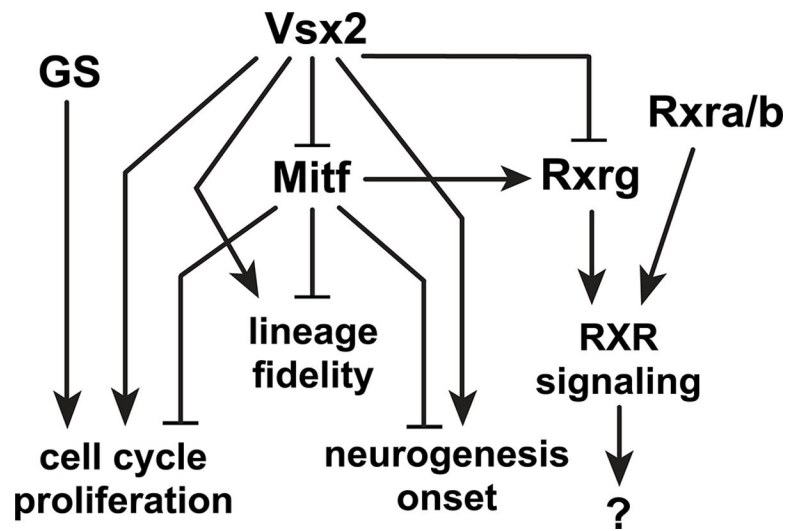
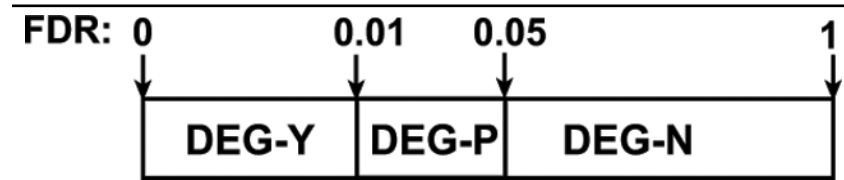


Figure 9: Summary of interactions.

Mitf is a central hub in the *Vsx2* interaction network, but other interactors are likely to contribute to the functions of *Vsx2* in mediating lineage fidelity, proliferation, and neurogenesis. *GS* activity converges with *Vsx2* to regulate RPC proliferation. How *RXR* signaling fits with *Vsx2* function is not clear, but our data predicts a minor role in the primary phenotypic traits of the early *orJ* retina.

Table 1:
DEG classifications based on *Vsx2*- and *Mitf*-dependencies.

(A) Two FDR cutoffs were used to assign all expressed genes to 3 categories based on their DEG status. The OvC comparison established regulatory dependencies on *Vsx2* and the OMvO comparison established regulatory dependencies on *Mitf*. The OMvO comparison was not informative at this level. Gene sets were defined based on *Vsx2* dependency. The number of genes in each DEG status group are shown.



The diagram illustrates the FDR cutoffs used for DEG classification. A horizontal bar is divided into three segments by vertical lines at FDR = 0.01 and FDR = 0.05. The segments are labeled DEG-Y (from FDR 0 to 0.01), DEG-P (from FDR 0.01 to 0.05), and DEG-N (from FDR 0.05 to 1). Arrows point down from the FDR values 0, 0.01, 0.05, and 1 to the corresponding vertical lines.

<u>comparison</u>	<u>DEG status</u>	<u>dependency</u>	<u>gene set</u>	<u>gene #</u>
<i>OvC</i>	<i>DEG-Y</i>	<i>Vsx2-Dep</i>	<i>V1</i>	5195
<i>OvC</i>	<i>DEG-P</i>	<i>Vsx2-poss Dep</i>	<i>V2</i>	1430
<i>OvC</i>	<i>DEG-N</i>	<i>Vsx2-Ind</i>	<i>V3</i>	7448
<i>OMvO</i>	<i>DEG-Y</i>	<i>Mitf-Dep</i>	<i>na</i>	949
<i>OMvO</i>	<i>DEG-P</i>	<i>Mitf-poss Dep</i>	<i>na</i>	485
<i>OMvO</i>	<i>DEG-N</i>	<i>Mitf-Ind</i>	<i>na</i>	12639
<i>OMvC</i>	<i>DEG-Y</i>	<i>na</i>	<i>na</i>	3386
<i>OMvC</i>	<i>DEG-P</i>	<i>na</i>	<i>na</i>	1378
<i>OMvC</i>	<i>DEG-N</i>	<i>na</i>	<i>na</i>	9309

Table 2:

Primary antibodies used for immunohistology.

Antibody	Species	Dilution	Source	Catalog #	RRID
Tubb3	Rabbit	1:10000	Biologends	802001	AB_2564645
Otx2	Rabbit	1:10000	Millipore	AB9566	AB_2157186
Rxrg	Rabbit	1:200	Santa Cruz	SC-555	AB_2269865

Author Manuscript

Author Manuscript

Author Manuscript

Author Manuscript

Table 3:

Small molecules used for retinal explant cultures.

Compound	Target	Vehicle	Source/Cat #	Working concentration
HX-531	Rxra, Rxrb, Rxrg	DMSO 0.1 % v/v	Tocris/188844-34-0	100 nM
DAPT	Gamma Secretase	DMSO 0.1 % v/v	Sigma/208255-80-5	1 – 5 μ M
DBZ	Gamma Secretase	DMSO 0.1 % v/v	Tocris/09984-56-5	300 nM – 1 μ M

Author Manuscript

Author Manuscript

Author Manuscript

Author Manuscript